An evaluation of NCRP report 151—radiation shielding design for radiotherapy facilities, and a feasibility study for 6 MV open-door treatments in an existing high-energy radiation therapy bunker

John Kildea, Ph.D

Master of Science

Medical Physics Unit

McGill University

Montreal, Quebec

February 2010

A thesis submitted to McGill University in partial fulfillment of the requirements of the degree of Master of Science in Medical Radiation Physics

ABSTRACT

This thesis describes a study of shielding design techniques used for radiation therapy facilities that employ megavoltage linear accelerators. Specifically, an evaluation of the shielding design formalism described in NCRP report 151 was undertaken and a feasibility study for open-door 6 MV radiation therapy treatments in existing 6 MV, 18 MV treatment rooms at the Montreal General Hospital (MGH) was conducted. To evaluate the shielding design formalism of NCRP 151, barrier-attenuated equivalent doses were measured for several of the treatment rooms at the MGH and compared with expectations from NCRP 151 calculations. It was found that, while the insight and recommendations of NCRP 151 are very valuable, its dose predictions are not always correct. As such, the NCRP 151 methodology is best used in conjunction with physical measurements. The feasibility study for 6 MV open-door treatments made use of the NCRP 151 formalism, together with physical measurements for realistic 6 MV workloads. The results suggest that, dosimetrically, 6 MV open door treatments are feasible. A conservative estimate for the increased dose at the door arising from such treatments is 0.1 mSv, with a 1/8 occupancy factor, as recommended in NCRP 151, included.

RÉSUMÉ

Ce mémoire décrit une étude des techniques de blindage utilisées dans les installations de radiothérapie pour des accélérateurs linéaires à mégavoltage. Plus précisément, une évaluation du formalisme de calcul de blindage tracée par le rapport NCRP 151 a été entrepris, et une étude de faisabilité a été menée avec le but de laisser la porte ouverte pour les traitements à 6 MV dans des salles de traitement déjà existantes à l'Hôpital général de Montréal (HGM). Pour évaluer le formalisme de blindage du NCRP 151, des doses équivalentes atténués par barrière ont été mesurés et comparés avec les résultats des calculs du NCRP 151. Cette étude a démontré que, même si les idées et recommandations du NCRP 151 sont très valables, ses prévisions de doses ne sont pas toujours correctes. En tant que tel, la méthode du NCRP 151 est mieux utilisée en conjonction avec des mesures physiques. L'étude de faisabilité pour des traitements de 6 MV à porte ouverte a utilisé le formalisme du NCRP 151, avec des mesures réalistes pour les charges de travail à 6 MV. Les résultats suggèrent que, dosimetriquement, les traitements de 6 MV à porte ouverte sont réalisables. Une estimation prudente pour la dose plus élevée à la porte découlant de ces traitements est 0.1 mSv, avec un facteur d'occupation de 1/8, comme recommandé dans le rapport du NCRP 151.

ACKNOWLEDGEMENTS

The completion of this research project would not have been possible without the generous support of many people. My supervisor Michael Evans has been a fantastic ally over the past few months. I am very grateful for the time he spent with me on this work and for the helpful advice and guidance he provided. I would also like to thank my co-supervisor Prof. Ervin Podgorsak for his financial support, encouragement and helpful editorial assistance.

My passage through the McGill Medical Physics program was facilitated by the excellent support of the Medical Physics Unit. I thank Dr. Jan Suentjens and William Parker for providing access to the facilities of the unit. Margery Knewstubb and Tatjana Nisic provided valuable help with all things bureaucratic. The didactic portion of the program was superb and I would like to express my gratitude to my teachers Waimed Abdel-Rahman, François deBlois, Slobodan Devic, Michael Evans, Georgi Hegyi, Christian Janicki, Pierre Leger, Shirley Lenhert, the late Ernst Meyer, William Parker, Horatio Patrocinio, Bruce Pike, Ervin Podgorsak, Andrew Reader and Jan Seuntjens.

My fellow students were both friends and teachers to me over the last year. We learned together and from each other. Sincere thanks to Saad Aldelaijan, David Giles, Joseph Holmes, Ileana Jelescu, Sangkyu Lee and Huriyyah Mohammed. My officemates Andrew Alexander, Tanner Connell and Eunah Chung provided great company over the last few months.

Beyond the realm of medical physics I have been blessed with a wonderful support network of friends. I thank my former astrophysics colleagues Trevor Weekes, David Hanna and Dave Fegan for their continued support and for many years of excellent mentoring. Amongst my friends in Montreal, Cesareo Loza Arciba deserves a special mention for his kind support over the last year and half. When things were tough he was always there to help. Jean Pichette and Grant Auer likewise. Jorge Gomez Lozano, Yann Helias and Hadi Karsoho have been great friends over the last few months. I am grateful to my fellow runners in Les Galopins for helping me stay fit and healthy and for literally keeping my feet on the ground, even when my head was in the clouds.

Finally and most importantly, I would like to thank my parents and family, who, as always, have supported and encouraged my education.

Go raibh maith agaibh go léir!

TABLE OF CONTENTS

LIST OF FIGURES

LIST OF TABLES

CHAPTER 1
Introduction

1.1 Overview of Thesis

This thesis describes two studies of radiation therapy shielding design carried out at the Montreal General Hospital (MGH). The first study entailed a general evaluation of the shielding design formalism outlined in the NCRP report 151. The second comprised a feasibility study for implementation of open-door 6 MV radiation therapy treatments at the MGH.

This chapter introduces the associated sciences of radiation therapy and radiation protection. Chapter 2 presents the physical processes encountered therein. Chapter 3 describes the shielding design formalism of the NCRP report 151–the internationally accepted standard for shielding design in radiation therapy. Chapters 4 and 5 detail the research undertaken in this project, the conclusions of which are developed in chapter 6.

1.2 Radiation Therapy and Radiation Protection—An Overview

As is the case for most medical procedures, radiation therapy is a double-edged sword. On the one hand, its effectiveness in treating cancer and several other diseases is well established (see section 1.5). On the other hand, the potential for radio-iatrogenesis, in the form of short- or late-term effects, both to the patient and to the therapist, is significant. Owing to the high levels of radiation used in the treatment of disease, radiation protection plays a vital role in modern radiation therapy departments.

1.3 Historical Perspective

Ionizing radiation has been used in medicine since the discovery of X rays in 1895 by the German physicist Wilhelm Konrad Röntgen. Röntgen's demonstration that X rays may be used to image the bony structures of the body marked the beginning of diagnostic radiology. The first therapeutic application of ionizing radiation, involving disappearance of a hairy mole treated with X rays, is believed to have been made by the Austrian surgeon Leopold Freund in 1896 (Hall and Giaccia, 2006). Today, over a century later, X-ray imaging has revolutionized diagnostic medicine, and radiation therapy is an increasingly important modality in the treatment of cancer and several benign lesions.

The science of radiation protection (also known as health physics) grew in parallel to developments in diagnostic radiology and radiation therapy. The earliest recorded biologic effects of radiation were reported within a year of Röntgen's discovery and included skin "burns", epilation and eye irritation (Hall and Giaccia, 2006). In 1915, the British Röntgen Society introduced the first formal proposals for radiation protection. A little over a decade later, in 1928, the British proposals were internationally adopted at the Second International Congress of Radiology in Stockholm. At the same congress, the International X-Ray and Radium Protection Committee (IXRPC) was established. Following World War II, the IXRPC was reconstituted as two separate commissions: the International Commission on Radiological Protection (ICRP) and the International Commission on Radiation Units and Measurements (ICRU), both of which still operate.

The US equivalent of the IXRPC was the Advisory Committee on X-Ray and Radium Protection, which operated from 1929 until the end of World War II. In 1946, it was replaced by the National Council on Radiation Protection and Measurements (NCRP), a non-governmental public service organization with a congressional charter to provide recommendations regarding radiation protection. NCRP reports form the basis of radiation protection policy within the United States and are consulted internationally for their scientific value.

In Canada, the Atomic Energy Control Board (AECB) was established under the Atomic Energy Control Act of 1946, with a charge to assist the Canadian government in matters pertaining to radiation in regulation, mining and research. In 2000, the Canadian Nuclear Safety Commission (CNSC) replaced the AECB. The commission's mandate is stipulated in the Nuclear Safety and Control Act of 1997 and it serves to regulate the use of nuclear energy and materials in Canada.

1.4 Disease

Cancer (malignant neoplasm) is a class of many diseases in which the cells within a tissue of an organism undergo uncontrolled division, intrude on nearby tissues, and sometimes metastasize (spread) to distant tissues. Most cancers form neoplastic tumors (lesions of cancer cells) but some, such as leukaemia, do not. Benign tumors are self-limited tumors that neither invade nor metastasize.

1.4.1 Cancer Microbiology

Human cells are either somatic or germline and they propagate by cell division. Somatic cells make up the tissues and organs of the body, whereas germ cells make up the gametes (spermatozoa and ova). Normal healthy tissue comprises somatic cells in homoeostasis—cell creation and cell death in equilibrium. Maintenance of homoeostasis is dependent upon regulated cell division (mitosis) and programmed cell death (apotosis). Any interruption in the regulation process may result in malignant progression from homoeostasis to metastasis and thus the development of cancer. Three groups of genes, proto-oncogenes, tumor-suppressor genes and DNA stability genes, regulate the division and death of somatic cells.

It is at the DNA-level that carcinogenesis manifests itself: DNA damage within the three groups of control genes may permit uncontrolled growth and cellular immortality. Carcinogenesis may occur spontaneously through random errors in DNA replication or may result from exposure to carcinogenic agents such as chemical mutagens, ionizing radiation, UV and viruses.

Cancer may affect people (and animals) of all ages, although the risk for most types of cancer increases with age. It is estimated (Canadian Cancer Society, 2009) that 40% of Canadian women and 45% of Canadian men will develop some form of cancer during their lifetime. According to the Canadian Cancer Society, 75 300 deaths due to cancer were expected in Canada during 2009. Indeed, the current cancer incidence in developed countries is about 5 000 new cancers per one million population, with the rate steadily increasing by some 3% per year.

1.4.2 Cancer Treatment

The goals of cancer treatment are complete removal of the tumor from the patient's body or palliative care. These goals are mainly achieved using three treatment modalities: (1) surgery (involving direct resection of the tumor), (2) chemotherapy (use of antineoplastic drugs) and (3) radiation therapy (use of ionizing radiation to kill tumor cells).

Some cancers may be treated with one treatment modality alone (radical treatment) but generally a combination of modalities (adjuvant treatment) is employed. Radiation therapy is used radically or adjuvantly depending on the type and location of the tumor, its grade (how aggressive it is), its stage (how advanced it is) and the general state of the patient. Worldwide, radiation is used to treat about 50% of all cancer patients, either as part of their primary treatment or in connection with recurrences or palliation (IAEA, 1998).

1.5 Modern Radiation Therapy

The purpose of radiation therapy is to deliver a prescribed dose of radiation to a target (typically a tumor) in a patient's body, conforming the dose with the 3-dimensional shape of the target and sparing surrounding healthy tissue from radiation damage. Following diagnosis of a tumor, a radiation oncologist may prescribe a dose of radiation to destroy the malignancy and a suitable treatment schedule (fractionation). The prescribed dose is based on medical precedence, the oncologists's experience and the patient's condition.

1.5.1 The Radiation Therapy Treatment Process

Detailed planning for the patient's treatment is the responsibility of the dosimeterist, while the treatment itself is administered by radiation therapists. The physician, dosimeterist, therapist, and most importantly the patient, all rely on an accurate and precise dose delivery system: the physical treatment process must deliver the prescribed dose to the tumor as prescribed and planned. Responsibility for the fidelity of the physical dose delivery falls to the medical physicist.

Three main types of radiation therapy are available, each distinguished by the location of the source of radiation employed. These are: (1) external beam radiation therapy (in which the source of radiation is external to the patient's body), (2) brachytherapy (in which the source of radiation is a temporary or permanently sealed radioactive source, or sources, placed directly into the region of the patient's body to be treated), and (3) unsealed source radiotherapy (in which the source of radiation is administered systemically by injection or ingestion).

The choice of one radiation therapy technique over another depends on a number of factors, such as the type, size and location of the tumor, the experience of the physician, the patient's condition, and the practicality of the technique. The majority of cancer patients (typically 80%) who are prescribed radiation are treated using external beam radiation therapy.

1.5.2 Beam Delivery in External Beam Radiation Therapy

The absorption of radiation dose within a medium (for example, a patient's body or phantom) may be described by a percentage depth dose curve (PDD). In a PDD distribution, the absorbed dose at a particular depth within the medium is plotted as a percentage of the maximum absorbed dose. The shape of the PDD depends on the beam type (photon or charged particle), beam energy (higher energy beams are more penetrating), and on the absorbing material (water, soft tissue, bone, etc). Several examples of typical PDD distributions are shown in Figure 1.1.

Photon beams for use in external beam radiation therapy are produced using either superficial or orthovoltage X-ray machines (10 kV[1] to 100 kV and 100 kV to 500 kV, respectively), cobalt teletherapy gamma-ray units (1.25 MeV) or linear accelerators (2 MV to 25 MV). Superficial and orthovoltage X rays are used to treat lesions on or close to the patient's skin. As such, the external photon beam is delivered from just one direction. Higher energy beams, used to deliver and conform the dose to deeper lesions, are

[1] The units kV (kilovoltage) and MV (megavoltage) refer to the kinetic energy, keV and MeV, respectively, of the electrons used to produce the corresponding X-ray beam. Since the X-ray beams used in radiation therapy are bremsstrahlung in nature, the kV or MV unit indicates the maximum energy of the photons that comprise the beam.

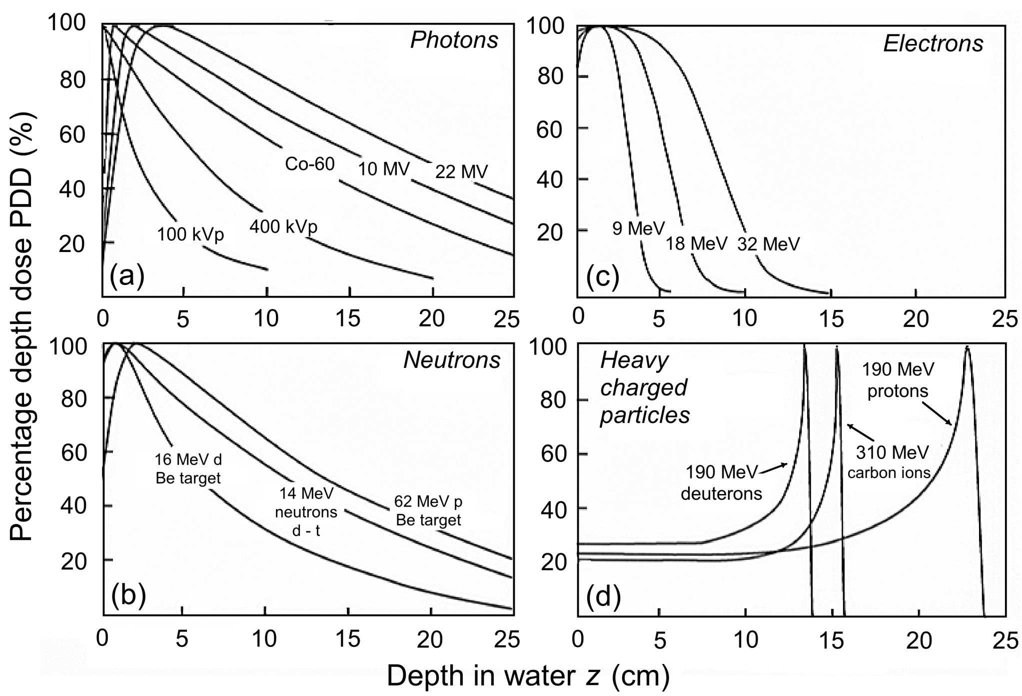

Figure 1.1: Percentage Depth Dose curves (PDDs) in water for various radiation beams used in radiation therapy. (a) photons, (b) neutrons, (c) electrons and (d) protons and heavy charged particles. Higher energy beams are more penetrating for all beam types. Figure from Podgoršak (2006), with permission.

Modality	Quantum	Beam	Source	Description
Superficial and orthovoltage therapy	X rays	Continuous	X-ray machine	Used to treat surface lesions
Teletherapy	Gamma rays	Continuous	Co-60	Source held in shielded container except during treatment
Conventional 3D XBRT	X rays	Pulsed	Linac	Conventional conformal external beam radiation therapy. Beams are delivered from many angles and intersect at tumor
Brachytherapy	Gamma rays	Continuous	Radioactive source	Employs radioactive sources inserted into patient
Electron therapy	Electrons	Pulsed	Linac	Used to treat lesions at or near surface
Proton therapy	Protons	Continuous	Synchrotron	Highly conformal 3D radiation therapy
IMRT	X rays	Pulsed	Linac	Intensity modulated radiation therapy. Beam shape is modulated to better conform with shape of tumor. Inverse treatment planning. Several beams used
RapidArc/VMAT therapy	X rays	Pulsed	Linac	IMRT-type treatment delivered in continuous arc (volumetric modulated arc therapy)
Tomotherapy	X rays	Pulsed	Linac	IMRT-type treatment with inbuilt imaging and helical beam delivery
SBRT	X rays	Pulsed	Linac	Stereotaxic body radiation therapy. Radiation therapy delivered in high-dose fractions with high spatial precision
IGRT	X rays	Pulsed	Linac	Image-guided radiation therapy. Patient repositioned prior to each fraction based on updated image of tumor
Gated RT	X rays	Pulsed	Linac	Patient motion (eg breathing) monitored and accounted for in beam delivery
Gammaknife SRS	Gamma rays	Continuous	Co-60	Stereotaxic radiosurgery using a dedicated Co-60 unit
Linac SRS	X rays	Pulsed	Linac	Stereotaxic radiosurgery. High-precision beam delivery with accurate patient positioning
Cyberknife therapy	X rays	Pulsed	Linac	Robotic radiation therapy with real-time imaging
TBI	X rays or gamma rays	Pulsed or continuous	Linac or Co-60	Total body irradiation
TSEI	Electrons	Pulsed	Linac	Total skin electron irradiation

Table 1.1: Some of the radiation therapy treatment machines and modalities encountered in modern medicine.

delivered over a range of angles. Accordingly, teletherapy units and linear accelerators (linacs) are typically arranged with the radiation source on a gantry that can rotate around the patient (isocentric setup).

Table 1.1 provides a cursory overview of several standard radiation therapy machines and treatment modalities encountered in modern medicine. The list is not exhaustive, rather it is intended to serve as reference for the topics encountered later in this dissertation.

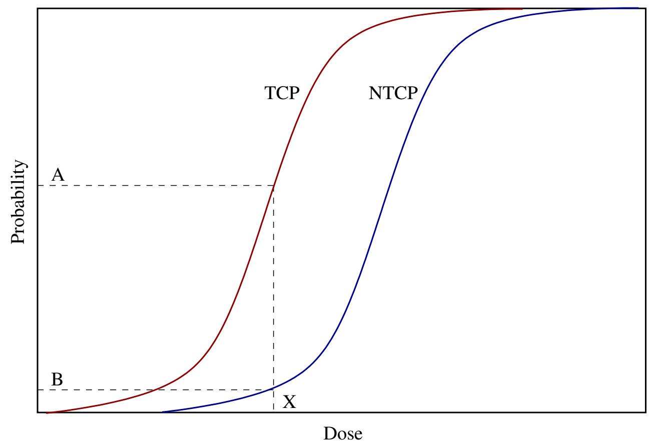

Figure 1.2: The dose response relationship for both the tumor (Tumor Control Probability) and surrounding healthy tissue (Normal Tissue Control Probability). The therapeutic ratio is the ratio of TCP to NTCP for a given dose. For dose X, the therapeutic ratio is A/B.

1.5.3 Basic Radiobiology of Radiation Therapy

Radiation therapy is effective in cancer treatment owing to the radiobiological consequences of the interaction of ionizing radiation with tumor cells. Due to their uncontrolled growth, tumor cells are frequently in a state of division; the state at which they are also the most radiosensitive. Following irradiation, cells die by a processes known as mitotic death—lethal damage to the cell's DNA caused by the radiation prevents successful cell division.

Delivery of radiation to a tumor necessarily involves exposure of healthy tissue to radiation and associated potential radiation damage (morbidity). The *therapeutic ratio* relates the tumor response (Tumor Control Probability) for a fixed level of normal-tissue damage (Normal Tissue Complication Probability), as shown in Figure 1.2.

Radiation therapy techniques that maximize the therapeutic ratio include fractionation, 3D treatment planning incorporating dose delivery using multiple radiation beams, and conformal dose delivery using shaped radiation beams. Table 1.2 provides a brief description of each technique.

Technique	Description
Fractionation	The prescribed dose is split into a series of small treatments in order to allow normal tissue time to repair itself between each treatment. The technique simultaneously allows oxygen to diffuse into the inner region of the tumor following radiation damage to the outer region. Oxygen diffusion is important since oxygen enhances the toxic effect of ionizing radiation.
Multiple beam, 3D treatment planning and dose delivery	By employing multiple radiation beams from multiple directions, that intersect at the location of the tumor, it is possible to ensure that the tumor receives a higher dose than the surrounding healthy tissue.
Conformal dose delivery	The more the delivered dose conforms to the target volume, the less the surrounding tissue is exposed and damaged. Conformality is achieved by shaping the radiation beam to the shape of the tumor.

Table 1.2: Techniques used to maximize the therapeutic ratio in radiation therapy.

1.6 Modern Radiation Protection

The use of radiation offers great benefits to society. These benefits are realized in medicine, industry and power generation. However, radiation may be detrimental to human health and its use necessarily involves management of risk so as to mitigate injury to the individual user, and to society in general. Radiation risk may be controlled but not eliminated; any use of radiation entails an associated non-zero risk. The goal of radiation protection is, thus, to minimize the risk while maintaining the overall benefit to society.

Numerous national and international organizations attempt to "balance" the risks and benefits of radiation usage. Foremost among these are the previously mentioned ICRP, ICRU and NCRP. These scholarly organizations analyze the risk-benefit relationship and make non-binding recommendations for radiation exposure limits. The role of regulation falls to national and regional organizations, such as the CNSC and Health Canada in Canada, Santé et Services Sociaux in Quebec, and the Nuclear Regulatory Commission (NRC) in the USA.

1.6.1 Radiation Dosimetry

In order to limit the exposure of individuals and society to radiation, such radiation exposure must be measurable and its biological effects quantifiable.

Radiation dosimetry is the science of measuring radiation exposure, while radiobiology is the science of understanding the biological effects of radiation. In health physics, a number of dosimetric quantities and units, encompassing aspects of both dosimetry and radiobiology, are defined. Table 1.3 outlines quantities and units that are most commonly used.

Absorbed Dose

The basic physical quantity that is used to measure the "amount" of radiation is the *absorbed dose* D. It is simply a measure of the energy of ionizing radiation absorbed per unit mass of absorbing material. The unit of absorbed dose is the gray (Gy).

Equivalent Dose

Since some radiations are biologically more effective (more dangerous) than others, the ICRP defined the quantity *equivalent dose* H which, for a particular tissue, is the absorbed dose multiplied by a radiation weighting factor W_{R}. The unit of equivalent dose is the sievert (Sv). The ICRP Publication 103 (2007) lists the ICRP's most recent recommendations for radiation weighting factors.

Effective Dose

The quantity *effective dose* E was defined by the ICRP to account for the variation in radiation sensitivity among the tissues and organs of the body. The effective dose is defined as the sum of the equivalent doses to exposed tissues and organs multiplied by the appropriate tissue weighting factors. The sievert is also the unit of effective dose.

Collective Effective Dose

In order to compare the effective doses between exposed population groups, the ICRP introduced the quantity *collective effective dose* S. The collective

Quantity	Definition	Formula	Unit
		Purely Physical	
Absorbed dose	Energy absorbed per unit mass	$D = \frac{\Delta E_{abs}}{\Delta m}$	Gray (1 Gy = 1 $\frac{J}{kg}$)
		Concerning Individuals	
Equivalent dose	Absorbed dose × radiation weighting factor for a particular tissue, T and radiation, R[a]	$H_T = w_R D_{T,R}$	Sievert (1 Sv = 1 $\frac{J}{kg}$)
Effective dose	Sum of equivalent doses to exposed tissues and organs, each multiplied by the appropriate tissue weighting factor	$E = \sum_T w_T H_T$ (for tissue T)	Sievert (1 Sv = 1 $\frac{J}{kg}$)
		Concerning Populations	
Collective effective dose	Product of average effective dose and the number of individuals exposed	$S = \sum_i \bar{E}_i N_i$ (for individuals i)	Person-sievert

[a] The radiation weighting factor is 1 for photons and electrons, 2 for protons and 20 for alpha particles and heavy nuclei. For neutrons, the weighting factor varies from 5, for thermal neutrons, to 20, for fast neutrons. See ICRP Publication 103 (2007) for full details of radiation and tissue weighting factors

Table 1.3: Dosimetric quantities and units used in radiation protection.

effective dose is defined as the product of the average effective dose to an exposed population and the number of persons exposed. The unit of collective effective dose is the person-sievert.

1.6.2 Background Radiation

In radiation protection, it is instructive to consider the level of background radiation, both natural and artificial, that society is exposed to. It provides a good indicator of what is “normal” and it can be used as a reference level when discussing radiation exposure.

Natural Background Radiation

Radiation is a natural part of the Earth’s environment and so it is ubiquitous and unavoidable. Natural background radiation is composed of cosmic radiation (from space), terrestrial radiation (from the soil and the rocks) and internal radiation (from the radioactive elements within our bodies). Our exposure to natural radiation is a function of our location on the Earth’s

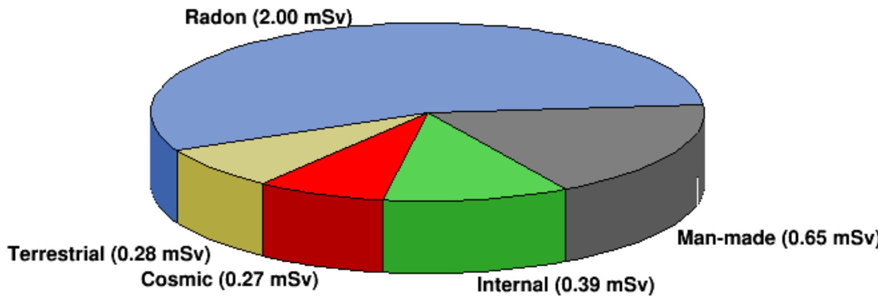

Figure 1.3: Breakdown of the estimated background radiation for a member of the population of the United States. Note: the corresponding effective dose values for Canada are estimated at approximately 20% lower. Data from NCRP Report 93 (1987).

surface—the abundance of radioactive elements varies over the Earth's surface and the cosmic ray flux increases with altitude and with distance from the equator.

Artificial Background Radiation

In addition to natural background radiation, modern society is exposed to radiation from artificial (man-made) sources. These include radiation exposure for medical purposes (Mettler et al., 2009), low-level radiation exposure from nuclear power plants and radiation exposure from consumer goods (such as smoke detectors and CRT TV screens). Figure 1.3 shows the distribution of the estimated background radiation for a member of the population of the United States (the corresponding effective dose values for Canada are estimated to be approximately 20% lower) (NCRP Report 93, 1987).

1.6.3 The Biological Effects of Radiation

When radiation is absorbed in biological tissues it can cause initial injury at the microscopic level. In some cases the microscopic damage may be repaired, in other cases, it may ultimately manifest itself macroscopically as an observable

Syndrome	Dose Range	Description
Hematopoietic syndrome	2.5 Sv to 5 Sv	Characterized by death of bone marrow due to sterilization of the bone marrow precursor cells. Without major intervention, the affected individual will die within weeks or months.
Gastrointestinal syndrome	5 Sv to 12 Sv	Involves depletion of the stem cells that generate the epithelium of the gut. Death is expected within days to weeks.
Cerebrovascular syndrome	Above 100 Sv	Involves breakdown of the neurologic and cardiovascular systems. Death occurs within hours of exposure.

Table 1.4: The three whole-body radiation sickness syndromes.

effect. The macroscopic biological effects of radiation can be divided into deterministic and stochastic effects.

Deterministic Effects

Deterministic effects of radiation are biological effects that increase in severity with increasing absorbed dose in an exposed individual. They have dose thresholds above which the effect will definitely occur, and below which it will not, as shown in Figure 1.4a. The threshold is specific to the exposed individual but average thresholds may be determined for a population. Examples of deterministic effects include radiation cataractogenesis, tissue fibrosis, organ atrophy and the syndromes of whole body radiation sickness.

Whole body radiation sickness occurs following acute high dose whole-body exposures. Three main syndromes are defined: the hematopoietic syndrome, the gastrointestinal syndrome and the cerebrovascular syndrome. Each is characterized by the dose range involved and the part of the body affected. Table 1.4 provides a brief summary of the three whole-body radiation sickness syndromes.

Stochastic Effects

Stochastic effects are biological effects in which the risk of the effect occurring, rather than its severity, increases with radiation dose, as shown in Figure 1.4b. Stochastic effects include radiation carcinogenesis and genetic effects.

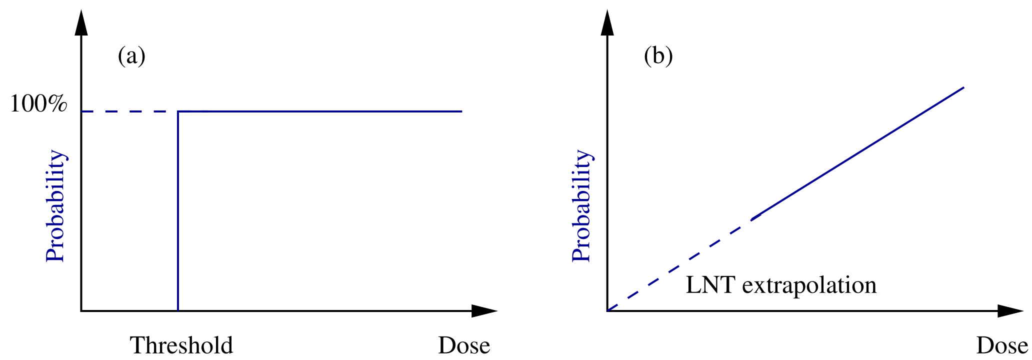

Figure 1.4: The probability of the biological effects of radiation against dose. (a) Deterministic effects have a threshold dose beyond which the probability of occurrence is 100% (b) Stochastic effects have no threshold. In the LNT model, the observed linear dose-dependence at high doses is extrapolated back to the origin.

Stochastic effects are probabilistic, do not have a threshold level, and apply to populations rather than individuals.

The *linear-no-threshold* (LNT) model is a model of the dose-risk relationship for stochastic biological effects. It makes an assumption that the linear increase in the probability of a stochastic effect, seen at high doses, can be extrapolated back to the low dose regime, indeed to the origin, as shown in Figure 1.4b. The no-threshold premise of the LNT model is controversial in that data relating to radiation effects at low doses are statistically compromised by low frequency and the presence of naturally-occurring spontaneous carcinogenesis. However, it is a usefully conservative model for use in radiation protection—it suggests that no dose level is safe and that exposure to ionizing radiation should be both minimized and justified.

1.6.4 Effects of In-utero Irradiation

The developing embryo is highly sensitive to ionizing radiation due to extensive cell division and rapid growth. Gestation may be divided into three main stages: pre-implantation (up to 9 days following conception), major organogenesis (2nd to 8th week after conception) and fetal growth (end of major organogenesis until term). Each stage is characterized by a different response to radiation.

At the pre-implantation stage, the conceptus, which is still a small number of undifferentiated cells, is generally affected in an all-or-nothing manner. Either the radiation causes fatal damage, or the cells survive. During major organogenesis, cellular differentiation and the formation of tissues and organs occurs. Each organ and tissue is most sensitive at the peak of its differentiation. The CNS appears to be particularly sensitive during major organogenesis and microcephaly was observed in the children born by Hiroshima survivors who were exposed at this stage. The final stage of development, fetal growth, appears to be the least sensitive to radiation, although behavioural alterations and reduced intelligence later in life have been observed. The biological effects of prenatal radiation were studied by the ICRP and reported in publication 90 (ICRP Publication 90, 2003).

1.6.5 Radiation Risk and Dose Limits

Given the existing data on the biological effects of radiation (mainly at high dose levels, derived from studies of Japanese atomic bomb survivors, occupationally exposed workers, and patients exposed for medical reasons) it is possible to estimate dose-risk relationships for both deterministic and stochastic effects. The ICRP and the NCRP have attempted to do so (ICRP Publication 103, 2007; NCRP Report 116, 1993) and have drawn up dose limit recommendations for occupationally exposed persons, pregnant workers and for the general public.

Occupational Exposure

The ICRP and NCRP occupational dose limits serve to: (a) limit the occupational dose to levels where deterministic effects are essentially avoided and

(b) limit stochastic effects such that the predicted risk is no greater than the average risk of accidental death for workers in safe[2] industries. The ICRP's effective dose limit for occupationally exposed workers, as recommended in the ICRP Publication 103 (2007) is 20 mSv per year, averaged over 5 years.

For declared pregnant workers, the ICRP recommends that the embryo/fetus should be provided with a level of protection broadly similar to that provided for members of the public. Thus, the pregnant worker should not exceed about 1 mSv for the remainder of the pregnancy.

Public Exposure

In the case of dose limits for members of the public, the ICRP and NCRP considered the general risks of accident and death encountered by the public and the level of natural background radiation that the public is exposed to ($\sim$1 mSv, or a mortality risk of 10^{-4} to 10^{-5}, when radon is excluded). Their recommended effective dose limit for the public is set at 1 mSv above the background level.

1.6.6 Canadian Regulations

In Canada, the CNSC has, for the most part, adopted the ICRP recommendations for occupational and public exposures. The CNSC's effective and equivalent dose limits[3] are listed in Table 1.5. The CNSC and ICRP differ in the effective dose limit for pregnant workers after declaration of pregnancy. Whereas the ICRP recommends 1 mSv for the remainder of pregnancy, the CNSC permits up to 4 mSv. Nevertheless, in accordance with the ALARA

[2] Safe industries are defined as having an annual fatal accident rate of 1 or less per 10,000 workers, ie an average risk of 10^4.

[3] CNSC dose limits are available online at: http://laws.justice.gc.ca/PDF/Regulation/S/SOR-2000-203.pdf

Organ/ Tissue	Person	Period	Dose (mSv)
		Effective Dose Limits	
Whole body	Nuclear energy worker, including a pregnant nuclear energy worker	(a) One-year dosimetry period (b) Five-year dosimetry period	50 100
	Pregnant nuclear energy worker	Balance of the pregnancy	4
	A person who is not a nuclear energy worker	One calendar year	1
		Equivalent Dose Limits	
Lens of an eye	(a) Nuclear energy worker	One-year dosimetry period	150
	(b) Any other person	One calendar year	15
Skin	(a) Nuclear energy worker	One-year dosimetry period	500
	(b) Any other person	One calendar year	50
Hands and feet	(a) Nuclear energy worker	One-year dosimetry period	50
	(b) Any other person	One calendar year	50

Table 1.5: CNSC effective and equivalent dose limits.

principle (see section 1.6.7, below), one would expect that, in any case, the pregnant worker should not approach the 4 mSv level.

1.6.7 The ALARA Principle

The ALARA principle is central to the concept of radiation protection. It stipulates that all/any exposure to ionizing radiation should be kept As Low As Reasonably Achievable, economic and social factors being taken into account—essentially a manifestation of the LNT model. In practical terms, it means that the use of radiation should not imply a level of exposure that approaches the regulatory limits. Rather, every effort should be made to ensure that the dose limits are never reached.

1.6.8 The Basic Physics of Radiation Protection

The three tenets underlying the physics of radiation protection are: distance, time, and shielding. Each is described below:

(1) Distance. The distance from the source should be maximized. The inverse-square law governs the fall-off in dose as a function of source distance; meaning that, for example, a doubling of the distance will reduce the exposure level by a factor of 4.

(2) Time. The duration of an exposure should be minimized, since the accumulated exposure increases linearly as a function of time.

(3) Shielding. The amount of shielding around the source should be maximized. The Beer-Lambert law governs the attenuation of a radiation beam through a barrier material—essentially dose falls off exponentially with distance through an attenuating material, the coefficient of attenuation depending on the material and the radiation.

1.6.9 Radiation Protection and Safety in Radiation Therapy

Radiotherapy, by definition, involves large doses of radiation. A radiation therapist would exceed his/her annual dose limit within a short period of time, if radiation protection measures were not in place. In Canada, radiation therapy facilities employing X-ray beams with energies exceeding 10 MV are classified as Class II nuclear facilities. Class II facilities operate under a license from the CNSC. Thus, the majority of radiation therapy facilities are subject to CNSC inspection and must demonstrate adherence to the CNSC dose limits for workers and members of the public.

Staff working in Class II medical facilities are often classified as Nuclear Energy Workers (NEWs) owing to the likelihood of them exceeding the public dose limit. Each NEW is issued with a TLD (thermoluminescent dosimeter) badge and accumulated exposure is recorded in the Canadian National Dose Registry[4] by Health Canada.

The three tenets of radiation protection are employed in the design of radiation therapy facilities (as is also the case for diagnostic radiology facilities). While use of distance is constrained by the facilities and the time is set by the

[4] The website for the National Dose Registry is: http://www.hc-sc.gc.ca/ewh-semt/occup-travail/radiation/regist/index-eng.php

schedules of the radiation therapists, the barrier thickness and composition may be designed as appropriate.

CHAPTER 2
Physical Processes of Significance in Medical and Health Physics

In nature, four distinct physical forces are observed. In decreasing order of strength, they are: the strong force (strength 1), electromagnetic force (strength $\frac{1}{137}$ of strong), weak force (strength $\sim 10^{-6}$ of strong) and gravitational force (strength $\sim 10^{-39}$ of strong). In addition, a number of associated elementary charged particles (and their anti-particles) are discernible. The elementary particles are those particles that are believed to have no substructure and thus cannot be broken down into smaller constituent particles. In particle physics theory, the elementary particles are considered either sources or carriers of the physical forces.

The Standard Model of particle physics incorporates the strong, electromagnetic and weak interactions plus the elementary particles that take part in those interactions. As yet, the model is unable to satisfactorily include the gravitational force. Three classes of elementary particle are found within the Standard Model: quarks, leptons and gauge bosons, as depicted in Figure 2.1. There are six known flavors (types) of quarks and six known types of leptons. Four gauge bosons have been experimentally observed (the four depicted in Figure 2.1), while a fifth, the Higgs boson, is predicted by the Standard Model but has eluded detection to date[1] .

[1] The search for the Higgs boson is the raison d'être of the Large Hadron Collider at European Organization for Nuclear Research (CERN) in Switzerland.

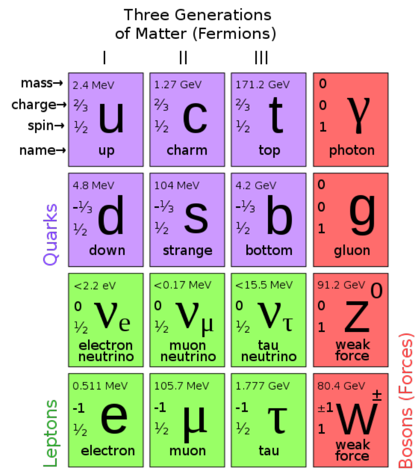

Figure 2.1: The Standard Model of particle physics. The three classes of elementary particle are depicted by color. The elementary fermions (six flavors of quarks and six types of leptons) are distinguished, together with the four elementary bosons that have been experimentally observed. Picture from Wikipedia entry on the standard model (wikipedia.org).

Each of the four fundamental forces are of interest to the medical physicist: The strong force (actually the residual strong force acting between nucleons) governs the binding energies of the nucleons; the weak force is responsible for beta decay; the electromagnetic force is behind all interactions that involve charged particles or photons; and the gravitational force is of practical importance in terms of its effects on mechanical systems.

2.1 Radiation

The term radiation has its origin in the Roman word radius, which was the name for the spoke of a wheel. Radii (or rays) pointed outward from the center of the wheel. Likewise, the term radius describes the distance from the center of a circle to its circumference. Radiation, in the modern sense, describes a stream of particles that emanate outward from a source. The particles may be elementary or composite and can be charged or uncharged. However, all radiating particles share the property that, as they move away from their source, they carry kinetic energy that was imparted to them at the source.

2.1.1 Ionization and Ionizing Radiation

An atom is the basic unit of matter. In the Rutherford-Bohr atomic model (Heilbron, 1981), an atom comprises a central, dense, positively charged nucleus containing nucleons (at least one positively charged proton and zero or more neutral neutrons) surrounded by a cloud of negatively charged electrons that are bound to the atom by the attractive positive charge of the nucleus. The electron cloud is arranged into discrete shells, with electrons in the inner shells being more tightly bound to the nucleus than those in the outer shells.

Under normal circumstances, the positive charge of the nucleus and the negative charge of the electrons balance one another making the atom neutral. However, if sufficient kinetic energy is given to a bound electron, it may overcome the attractive electromagnetic force of the nucleus and escape the atom, leaving behind a shell vacancy. The process of electron escape is known as ionization and an ionized atom is called an ion. The energy required to eject an electron from an atom is known as the electron's binding energy. Electronic binding energies are quantized according to atomic shell. The ionization potential of an atom refers to the energy of its least bound electron, i.e., the minimum energy needed to eject an electron from the atom. Ionization potentials range from a few electron volts for the alkali elements to 24.6 eV for helium.

Radiating neutral or charged particles with sufficient kinetic energy to eject electrons from the matter they encounter are called ionizing radiation. The process of ionization is either direct or indirect. Direct ionization results from the interaction of charged particles with matter (also called Coulomb interactions). Indirect ionization happens when a neutral particle interacts with matter to produce a charged particle that in turn causes ionization. Radiation carries energy (the kinetic energy of the charged particles) and through the process of ionization, the energy of the radiating particles is deposited in matter through which they pass (indirect ionization).

There are eight methods through which ionization (i.e., the production of an atomic shell vacancy) may occur. Three of them (photoelectric effect, Compton scattering, and triplet production) involve photons impinging on the atom, three others are the result of internal rearrangements amongst the atomic electrons or within the nucleus (Auger effect, electron capture, internal conversion) and two arise from charged particles incident on the atom (Coulomb interaction, positron annihilation). All are of interest to the medical physicist. In radiation therapy physics, the photon interactions and the Coulomb as well as Auger interactions are most frequently encountered; electron capture and internal conversion are important processes in nuclear medicine.

2.2 Photon Beam Attenuation

As a photon beam penetrates into a material (absorber), the photons may interact with the atoms of the material in a number of ways. They may interact with the nucleus (photodisintegration or pair production), with loosely bound[2] orbital electrons (Thomson effect, Compton effect, triplet production), or with tightly bound[3] orbital electrons (Rayleigh scattering, photoelectric effect). The photon is either absorbed completely in the interaction (photodisintegration, photoelectric effect and pair/triplet production) or it survives, either with the same energy and a different trajectory (Rayleigh scattering) or

[2] A loosely-bound orbital electron is one whose binding energy is much less than the incident photon energy.

[3] A tightly-bound orbital electron is one whose binding energy is comparable to or greater than the incident photon energy.

Interaction	Photoelectric Effect	Rayleigh Scattering	Compton Effect	Pair Production	Photo-disintegration
Photon interacts with	Atom as a whole	Atom as a whole	Free electron	Nuclear Coulomb field	Nucleus
Interaction mode	Photon disappears	Photon scattered	Photon scattered	Photon disappears	Photon disappears
Energy dependence	$\frac{1}{(h\nu)^3}$	$\frac{1}{(h\nu)^2}$	Decreases with energy	Increases with energy above threshold	Increases with energy above threshold
Threshold energy	Shell binding energy	None	Shell binding energy	$\sim 2m_ec^2$	Binding energy of nucleons
Linear attenuation coefficient	τ	σ_{R}	σ_{C}	κ	σ_{PN}
Z-dependence of mass attenuation coefficient	$\frac{\tau}{\rho} \propto Z^3$	$\frac{\sigma_{\mathrm{R}}}{\rho} \propto Z$	Independent of Z	$\frac{\kappa}{\rho} \propto Z^2$	Resonance peak decreases from about 23 MeV for Z >12
Particles released in interaction	Photoelectron	None	Recoil electron	Electron-positron pair	Photoneutron
Energy region of significance for water	<20 keV	<20 keV	20 keV-10 MeV	>10 MeV	>10 MeV
Energy region of significance for concrete	<100 keV	<100 keV	>100 keV	>10 MeV	>10 MeV
Energy region of significance for lead	<500 keV	<100 keV	500 keV-3 MeV	>3 MeV	>10 MeV

Table 2.1: Main properties of the photoelectric, Rayleigh, Compton, pair production and photodisintegration interaction processes for photons.

with reduced energy and a different trajectory (Compton effect). Any energy lost by the photon is ultimately emitted by the atom in the form of new photons or ejected electrons (the Auger effect, as described in section 2.4 below) as the ionized atom returns to a stable state.

The photon beam attenuation processes are summarized in Table 2.1 and described in detail below.

2.2.1 The Linear Attenuation Coefficient

The linear attenuation μ is described as the probability per unit path length that a photon will have an interaction with the material through which it

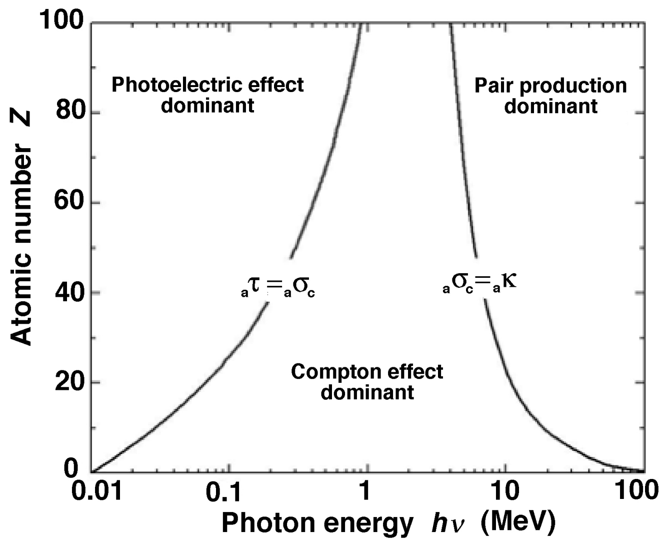

(a) Regions of relative photon interaction predominance. Figure from Podgoršak (2006), with permission.

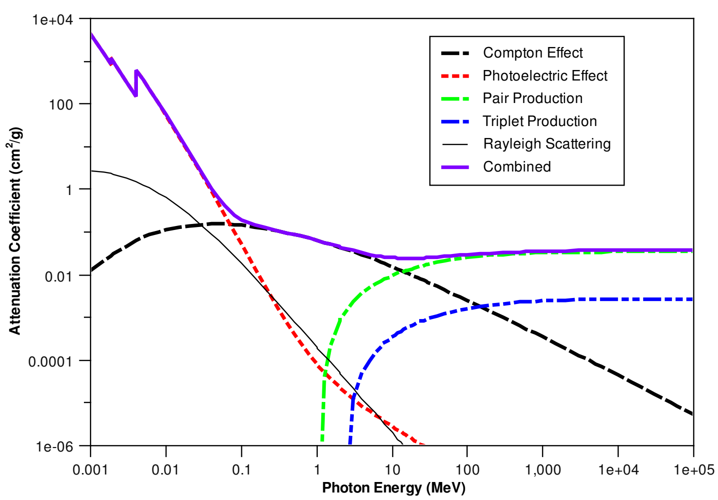

(b) Mass attenuation coefficients in concrete (tricalcium silicate).

Figure 2.2: Photon interactions, in general and in concrete (tricalcium silicate). Data from the NIST Photon Cross Sections Database.

is passing. It depends both on the energy of the photon and on the atomic number Z of the material. The Beer-Lambert law governs the exponential attenuation of a photon beam as it passes through an absorbing material. In terms of μ, the Beer-Lambert law may be expressed as

$$I(x) = I(0)e^{-\mu x}, \tag{2.1}$$

where $I(x)$ is the intensity of the photon beam at depth x in the material and $I(0)$ is the incident intensity.

The linear attenuation coefficient is normally determined using narrow-beam geometry, in which the beam under study arises from a narrowly collimated source. Although narrow beams are seldom encountered in applied radiation physics, they are practically useful, since they are more reproducible than broad beams.

A linear attenuation coefficient is defined for all photon interaction types, with the overall coefficient μ equalling the sum of the individual coefficients:

$$\mu = \sigma_{\mathrm{R}} + \tau + \sigma_{\mathrm{C}} + \kappa_{\mathrm{p}} + \kappa_{\mathrm{t}} + \sigma_{\mathrm{PN}} \tag{2.2}$$

where

- σ_{R} is the attenuation coefficient for Rayleigh scattering
- τ is the attenuation coefficient for the photoelectric effect
- σ_{C} is the attenuation coefficient for Compton scattering
- κ_{p} is the attenuation coefficient for pair production
- κ_{t} is the attenuation coefficient for triplet production
- σ_{PN} is the attenuation coefficient for photodisintegration

Figure 2.2(a) shows the regions of relative predominance of the three main interaction processes (photoelectric effect, Compton effect, nuclear pair production), while Figure 2.2(b) presents, as an example, the mass attenuation coefficient as a function of energy for a photon beam in tricalcium silicate (the main constituent of concrete). The mass attenuation coefficient for a particular material is equal to the linear attenuation coefficient for that material divided by its density. The mass attenuation coefficient essentially removes the density dependence of the linear attenuation coefficient.

2.2.2 Photoelectric Effect

The photoelectric effect is an interaction between a photon of energy $h\nu$ and a tightly bound orbital electron of an absorbing atom. Since the electron is tightly bound, the interaction occurs between the photon and the atom as a whole. In the process, the electron is ejected from the atom and is referred to as a photoelectron.

The only necessary condition on a photon ejecting a photoelectron is that the photon's energy must exceed the binding energy of the electron. Once unbound, the photoelectron carries away the energy difference as its kinetic energy:

$$E_{\mathrm{K}} = h\nu - E_{\mathrm{B}} \tag{2.3}$$

where

- E_{K} is the kinetic energy of the photoelectron
- $h\nu$ is the incident photon energy
- E_{B} is the electron binding energy in the atom

Following emission of a photoelectron, the remaining electrons in the atom reorganize themselves to fill the shell vacancy left behind. In the process, one or more characteristic photons and/or Auger electrons are emitted according to the fluorescence yield of the absorber (see section 2.4 below). The average energy transferred to electrons in a photoelectric interaction is given by:

$$\overline{E}_{\text{tr}}^{\tau} = h\nu - \sum_n P_n \omega_{\text{n}} \overline{h\nu_n} \tag{2.4}$$

where

- $\overline{E}_{\text{tr}}^{\tau}$ is the average energy transferred to electrons in the photoelectric interaction.
- $h\nu$ is the incident photon energy.
- P_n is the probability of the photoelectric effect occurring in the nth shell, if it occurs at all.
- ω_n is the fluorescence yield for the nth shell
- $\overline{h\nu_n}$ is the nth-shell weighted mean value of all possible fluorescence transition energies (typically ~90% of $E_{\text{B}}(K)$ for the K shell).

Any of the orbital electrons may be ejected as photoelectron. However, in medical physics, only those electrons in the inner (K and L) shells of high-Z materials are of importance—only such tightly-bound electrons have binding energies within the X-ray range. The photoelectric mass attenuation coefficient τ is proportional to Z^4 for low Z absorbers and to Z^3 for high Z absorbers. As shown in Figure 2.2, at diagnostic energies (below 100 keV), the photoelectric effect is the dominant photon interaction process.

2.2.3 Compton Effect

In the Compton effect, a photon interacts with a loosely bound orbital electron. The interaction results in a recoil electron and a scattered photon. Energy and momentum are conserved in the interaction, with the scattered photon and the recoil electron sharing the kinetic energy of the primary photon. The energy distribution is determined by the energy of the primary photon and the emission angle of the scattered photon.

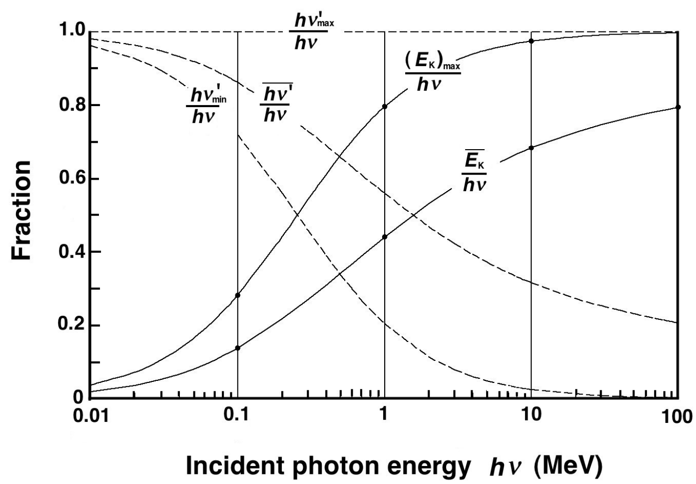

Figure 2.3: Average, maximum and minimum fraction of the incident photon energy $h\nu$ transferred in the Compton effect to the recoil electron E_{K} and to the scattered photon $h\nu'$.

The mass attenuation coefficient for the Compton effect σ_{C}/ρ is independent of the atomic number Z of the material. As shown in Figure 2.3, the average fraction of the incident photon energy $h\nu$ transferred to the recoil electron increases with $h\nu$. The Compton effect is the predominant photon interaction process in the energy range from ∼100 keV to ∼10 MeV.

2.2.4 Pair Production

Pair production occurs when a photon, with energy greater than twice the electron rest mass energy (1.022 MeV), is converted into an electron-positron pair in the presence of a third particle[4] . The third particle is needed to absorb the excess momentum from the photon that is not taken up by the electron-positron pair. The effect can happen in the presence of a nucleus (referred to as nuclear pair production), an orbital electron (known as electronic pair

[4] Pair production of a photon into a muon or tauon pair is also possible but at high photon energies available only in extreme environments such as particle colliders and in the cosmos.

production or triplet production), or another photon (also just referred to as pair production)[5] . Pair production by photons in the absence of matter but in the presence of superstrong magnetic fields ($> 10^{12}$ G) is theoretically possible and may help explain the emission signature of gamma-ray photons from intense astrophysical environments, such as pulsars (Daugherty and Harding, 1983).

The threshold for pair production is $\sim 2m_{\mathrm{e}}c^2$ and the threshold for triplet production is $4m_{\mathrm{e}}c^2$. Above the threshold, the mass pair production coefficient κ_{p}/ρ varies linearly with the atomic number Z of the absorber. The average energy transferred from the incident photon to charged particles in the pair production process is:

$$\overline{E}^{\kappa}_{\mathrm{tr}} = h\nu - 2m_{\mathrm{e}}c^2, \tag{2.5}$$

where

- $\overline{E}^{\kappa}_{\mathrm{tr}}$ is the average energy transferred to charged particles, and
- $m_{\mathrm{e}}c^2$ is the rest mass energy of the electron.

2.2.5 Photodisintegration

At energies above ∼10 MeV, photodisintegration (also known as the photonuclear interaction or nuclear photoelectric effect) is energetically feasible. In the photodisintegration interaction a photon is absorbed by a nucleus and the most likely outcome is release of a single photoneutron, through the (γ, n) reaction. Release of other charged particles, gamma rays, fission products or additional neutrons is also possible but much less likely.

[5] Pair production of one photon in the presence of another is very rare and is only favourable in intense astrophysical environments with high photon densities or over cosmological distances.

The cross section for the photodisintegration interaction is distinguished by the so-called "giant resonance" peak. The peak is broad (from 3 MeV to 9 MeV full-width-half-maximum) and is centered at about 24 MeV for low-Z absorbers and at about 12 MeV for high-Z absorbers. Two exceptions are the interactions ^{2}H(γ,n)^{1}H and ^{9}Be(γ,n)2α, which have giant resonance peaks at much lower energies. Apart from the two exceptions, the giant resonance peak energy steadily decreases from 24 MeV, for carbon-12, with increasing Z. The threshold energy for the photodisintegration interaction corresponds to the binding energy of the nucleons in the nucleus (about 8 MeV per nucleon, except for ^{2}H and ^{9}Be, for which it is 1.1 MeV/nucleon and 1.67/nucleon MeV, respectively).

Compared to the other photon interactions processes, the atomic cross section for photodisintegration σ_{PN} is relatively small. Even at the resonance peak energy it only amounts to a few percent of the total cross section. Accordingly, it is often neglected in photon interaction studies in medical physics. However, with regard to shielding considerations for high–energy (>10 MeV) linear accelerators, the photodisintegration interaction is of major importance. Photoneutrons released by the (γ,n) reaction are usually more penetrating than the photons that produce them. Additionally, the daughter nuclei resulting from the reaction may be radioactive and the photoneutrons may subsequently react with surrounding material through neutron capture. Indeed, photodisintegration-induced radioactivity is the reason why, in Canada, high-energy radiation therapy machines are classified as Class II nuclear equipment and are controlled by the CNSC.

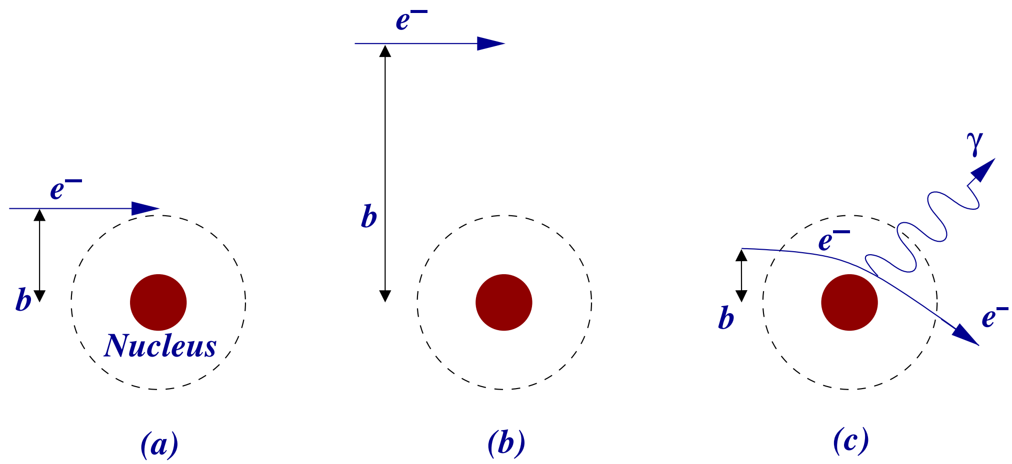

Figure 2.4: Collision types in the Coulomb interaction: (a) Hard collision, in which the impact parameter b is of the order of the atomic radius, (b) Soft collision, in which $b \gg a$, and (c) Radiation collision, where $b \ll a$.

2.3 Coulomb Interaction

Electrons and other charged particles interact through Coulomb interactions. Coulomb interactions are either collisional or radiative. In collision interactions (also known as ionization interactions), the charged particle energy is lost to the absorbing medium, whereas in radiation interactions it is lost to bremsstrahlung photons. Collision losses occur when the incident charged particle interacts with orbital electrons. Collisions can be hard (impact parameter of the order of the atomic radius) or soft (impact parameter much greater than the atomic radius). Hard collisions result in an ionized target atom, whereas soft collisions cause atomic excitation. Radiation loss occurs when the incident charged particle is decelerated by the Coulomb field of the target nucleus. Hard, soft and radiation collisions are illustrated in Figure 2.4.

2.3.1 Stopping Power

The energy lost by a charged particle in a Coulomb interaction is generally small (up to a maximum of $E_\mathrm{K}/2$ for electrons, where E_K is the kinetic energy of the electron), such that a particle can undergo many interactions before expending all of its energy. The gradual slowing down of a charged particle as it traverses an absorber is governed by the stopping power of the particle in the absorber.

The linear stopping power of a medium S is defined as the rate of kinetic energy loss per unit path length of a charged particle passing through it. The mass stopping power S/ρ is equal to the linear stopping power S divided by the density ρ of the medium.

The total linear stopping power S_{tot} of a medium is a combination of its radiation and collision stopping powers, i.e.,

$$S_{\text{tot}} = S_{\text{rad}} + S_{\text{col}} \tag{2.6}$$

The mass collision stopping power of a medium for a particular charged particle is proportional to the square of the particle charge and inversely proportional to the square of its velocity. Accordingly, the rate of energy loss, the ionization of the medium, and the dose deposited in it, all increase as the particle slows down. This property is clearly demonstrated in Figure 1.1(d), which shows the percentage depth dose in water for heavy charged particle beams as a function of depth: as the particle travels through the medium, the dose increases slowly at first and then rapidly toward the end of its range, before dropping to zero. The peak at the end of the range is known as the Bragg peak. It is much more pronounced for protons and heavy charged particles than for electrons, since electrons suffer multiple scatterings en route that heavier particles do not.

2.3.2 Bremsstrahlung Yield

The bremsstrahlung yield B for a charged particle is defined as the fraction of the particle's initial kinetic energy that is emitted in the form of bremsstrahlung photons arising from radiation collisions. Owing to their momentum, heavy charged particles moving through a medium are deflected only very slightly by the Coulomb attraction or repulsion of a nucleus. Accordingly, the bremsstrahlung yield for heavy charged particles is negligible. For electrons, on the other hand, the bremsstrahlung yield can be as much as 1.0 and may be determined from stopping power data using the relation

$$\begin{aligned} B(E_{\mathrm{K}_0}) &= \int_0^{E_{\mathrm{K}_0}} \frac{S_{\mathrm{rad}}(E)}{S_{\mathrm{tot}}(E)} \mathrm{d}E \Big/ \int_0^{E_{\mathrm{K}_0}} \mathrm{d}E \\ &= \frac{1}{E_{\mathrm{K}_0}} \int_0^{E_{\mathrm{K}_0}} \frac{S_{\mathrm{rad}}(E)}{S_{\mathrm{tot}}(E)} \mathrm{d}E \end{aligned} \tag{2.7}$$

where E_{K_0} is the initial kinetic energy of the incident electron.

2.3.3 Range and Path of Charged Particles

The range R of a charged particle in a medium is the depth in the medium to which it travels before loosing all of its kinetic energy. The range depends on many factors, including the mass, charge, and kinetic energy of the particle and the composition of the medium. The path length l of a charged particle is the total distance travelled by it before it has lost all of its kinetic energy. For heavy charged particles which suffer few deflections R and l are approximately equal. For electrons, l is often considerably longer than R (up to twice as long), since the electron can undergo numerous interactions and large-angle deflections (scattering) before coming to rest.

2.4 The Auger Effect and Fluorescence Yield

The Auger effect refers to the emission of a second electron from an atom in the aftermath of an initial ionization event. Whenever a vacancy is created in an inner shell, the atomic electrons rearrange themselves to fill the vacancy and thereby move the vacancy to the outer shell. Excess binding energy between

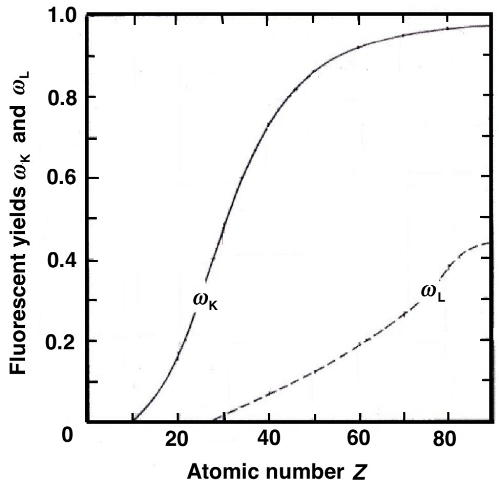

Figure 2.5: Fluorescence yields for the K and L shells, ω_K and ω_L respectively.

the initial and final shells of any rearranged electrons is normally emitted by the atom in the form of characteristic photons. However, on occasion the excess energy may be emitted as electrons (the Auger effect).

The fluorescence yield ω for a given shell in an atom gives the probability for the emission of a characteristic photon from the atom following an ionization event. The probability for the Auger effect is thus $1 - \omega$. Figure 2.5 presents a plot of the fluorescence yield and Auger probability for the K shell.

Fluorescence yield is important in the production of characteristic X rays at diagnostic X-ray energies, for example in mammography. It is also considered when calculating dose due to ionizing photons when the photoelectric effect is involved, as described in section 2.2.2.

2.5 Protons and Heavy Charged Particles

Energetic protons and heavy charged particles penetrating an absorber behave in a similar fashion to electrons, except that they carry greater momentum and so undergo little or no radiation loss. Owing to their greater mass, they also lose relatively little energy in each individual collision and may, as a result, travel deeper into a material before the Bragg peak occurs. This fact is exploited in proton and heavy-charged-particle therapy in order to deliver dose to a target volume with considerable sparing of surrounding healthy tissue (Schulz-Ertner and Tsujii, 2007).

2.6 Neutrons

Neutrons are indirectly ionizing particles that interact through nuclear interactions. Dose deposition by neutron beams is a two step process in which (a) the neutrons produce charged particles by nuclear interactions and (b) the charged particles deposit dose by Coulomb interactions. Both thermal neutrons ($E_{\mathrm{K}} \simeq 0.025$ eV) and fast neutrons ($E_{\mathrm{K}} > 0.1$ MeV) have applications in medicine. Thermal neutrons are used in boron-neutron capture therapy (BNCT) and fast neutrons are used in external beam radiation therapy.

There are five main processes through which neutrons may interact with matter. They are elastic and inelastic scattering, neutron capture, spallation and fusion. The first three are of most interest in radiation therapy physics and have application in the moderation and absorption of neutrons within the shielding of high-energy radiation therapy installations.

The production, interaction, and dose deposition of neutrons are important considerations in external beam radiation therapy involving photon beams of energy greater than $\sim$10 MeV. The production of neutrons in such beams by photodisintegration gives rise to additional neutron dose within the patient and a diffuse neutron beam within the treatment room that must be considered when designing the room's shielding. Shielding requirements for secondary neutrons are discussed in section 3.7.2.

2.7 Dose Deposition by Ionizing Radiation Beams

An ionizing particle (photon or charged particle) rarely imparts all of its energy to a material at once. Generally, it undergoes one or more ionization interactions and produces multiple secondary electrons that distribute its energy within the material.

The cascade process, through which a single primary particle gives its energy to a shower of secondary particles, is encountered in many areas of physics; including cosmic ray physics, particle physics and nuclear physics. Energy deposition starts with the primary particle, builds up to a maximum number of particles (shower maximum), and then fades away as the energies of the secondary particles fizzle out. Figure 2.6(a), depicts a Monte Carlo simulation of an air shower produced when a primary cosmic gamma-ray interacts with the earth's upper atmosphere (Kertzman and Sembroski, 1994). Indeed, similar Monte Carlo algorithms are often used to study particle showers in medical physics, particle physics and cosmic-ray physics.

In medical physics, particle showers are usually studied in terms of dose deposition in a water phantom. Dose deposition in water is a very important beam characteristic, since human tissue may be approximated to water. Figure 2.7 shows the PDD shape for a photon beam in water. Actual PDDs were presented previously in Figure 1.1. Three curve regions are thus defined: the build-up region, the depth of maximum dose and the decay (dose fall-off) region.

The water phantom can be considered as a composite of layers through which the primary particles and secondary electrons pass. Since dose is proportional to electron fluence, if one were to consider the PDD for a single particle entering a phantom, the depth of maximum dose would correspond to shower maximum. However, a radiation beam comprises a stream of primary

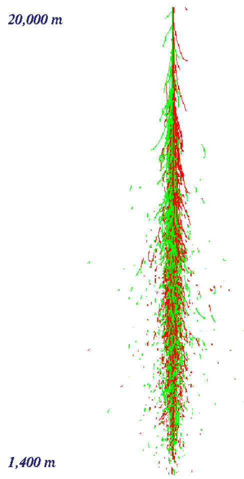

(a)

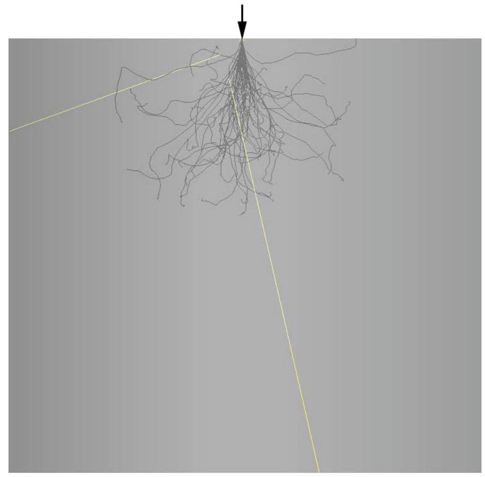

(b)

Figure 2.6: Particle showers, in air and in water. (a) Monte Carlo simulation of an air shower produced by a 500 GeV gamma-ray incident on the Earth's atmosphere. Depth is above sea level. Figure courtesy of G. Sembroski. (b) Monte Carlo simulation of an electron cascade in a 1 cm water phantom, resulting from 50, 1 MeV electrons. The arrow shows the location of the impinging electron beam, the black lines represent the electron tracks and the white lines represent bremsstrahlung photons. Figure courtesy of J. Seuntjens.

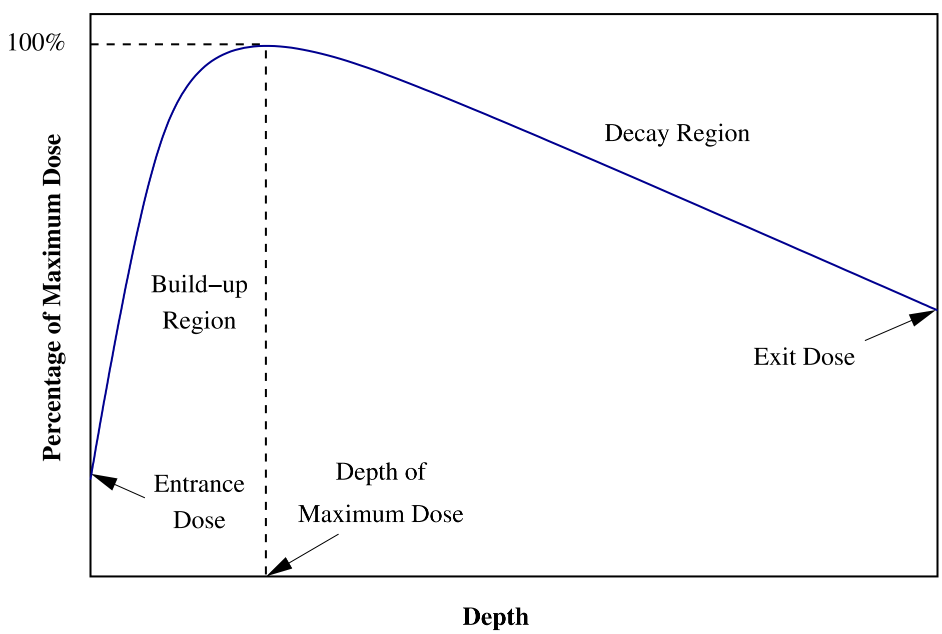

Figure 2.7: Generic shape of a photon PDD in water.

particles. As such, the PDD shape for a radiation beam is governed not only by the depth of shower maximum for the showers arising from each individual primary but also by the probability distribution (Beer-Lambert law) that describes the depth distribution over which the primaries interact. Furthermore, radiation initially scattered out of the beam may be scattered back into it, thereby moving shower maximum to a greater depth than would otherwise be expected.

In summary, the shape of a PDD is dictated by the combination of three processes (1) the Beer-Lambert, describing the depth at which each primary particle interacts (2) the overlapping electron showers instigated by each primary interaction and (3) the contribution to the beam of radiation originally scattered out of it.

2.8 The Buildup Effect

The build-up effect, in contrast to the build-up region, refers to the increase in flux measured at a point in an absorber-attenuated radiation beam as the beam width is increased. It is an important effect that must be accounted for in the design of shielding for radiation therapy facilities. Essentially, as illustrated in Figure 2.8, as the width of a radiation beam is increased, an increasing flux of radiation that was not originally emitted in the direction of the measurement point may be scattered to it.

The build-up factor B for a beam of radiation is defined as the ratio of its broad beam intensity to its narrow beam intensity, measured at the same point within the beam:

$$B = \frac{I_B(x)}{I_N(x)} \tag{2.8}$$

where

- $I_B(x)$ is the broad beam intensity measured at point x, and

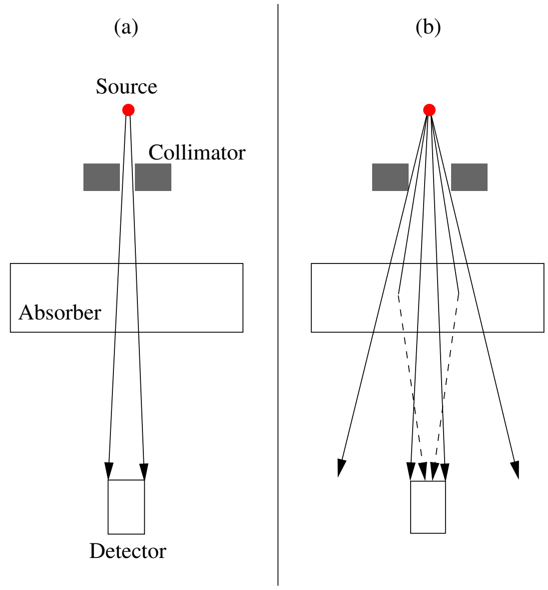

Figure 2.8: Illustration of the buildup effect. As the width of an absorber-attenuated radiation beam is increased, an increasing amount of scattered radiation may reach the detector. In (a) the beam is collimated to give narrow beam geometry, while in (b) the collimator is opened for broad beam geometry. In (a) only primary radiation (solid lines) reaches the detector, whereas in (b) both primary and scattered radiation (dashed line) are detected.

- $I_N(x)$ is the narrow beam intensity measured at point x.

2.9 Radiation Detectors and Dosimeters

The purpose of a radiation detector is to produce a signal in proportion to the flux of radiation passing through it. The signal produced depends on the interaction between the radiation and the detection medium. A radiation dosimeter is a radiation detector that measures, either directly or indirectly, the dosimetric quantities exposure, kerma, absorbed dose or equivalent dose, or their time derivatives. This project employed two types of radiation detector: gas-filled detectors and TLDs. All were used as dosimeters to measure equivalent dose. A short description of each type is provided here.

2.9.1 Gas-Filled Detectors

Gas-filled detectors comprise a volume of insulating gas contained between two electrodes having a voltage difference between them. In the absence of ionizing radiation, current cannot flow through the gas and the detector acts as a capacitor. Upon passage of ionizing radiation through the detector, electrons and ions will be produced in the gas and will be attracted to the electrodes resulting in a measurable electrical current.

As shown in Figure 2.9, a gas-filled detector may operate in a number of regions depending on the relationship between the voltage applied and the charge collected[6] . Indeed, gas-filled detectors are categorized according to the voltage region in which they operate.

No detectors operate in the *recombination region* (A) or in the *gas discharge region* (E). In the low-voltage recombination region, the electrical potential is insufficient to collect all charges produced in the gas before they recombine. In the high-voltage gas discharge region, the voltage is sufficiently high that a single ionizing event may initiate a continuous discharge, thereby rendering the detector useless.

Ionization Chambers

At voltages above the saturation voltage V_s, the potential is more than sufficient to collect all charges produced in the chamber's sensitive volume and the detector operates in the *ionization chamber* or *saturation* region (B). No charge multiplication occurs in this region and the charge collected is directly proportional to the number of primary ions (of either sign) produced by the radiation.

[6] Note that no single ionization chamber can be taken through all of the five regions shown in Figure 2.9.

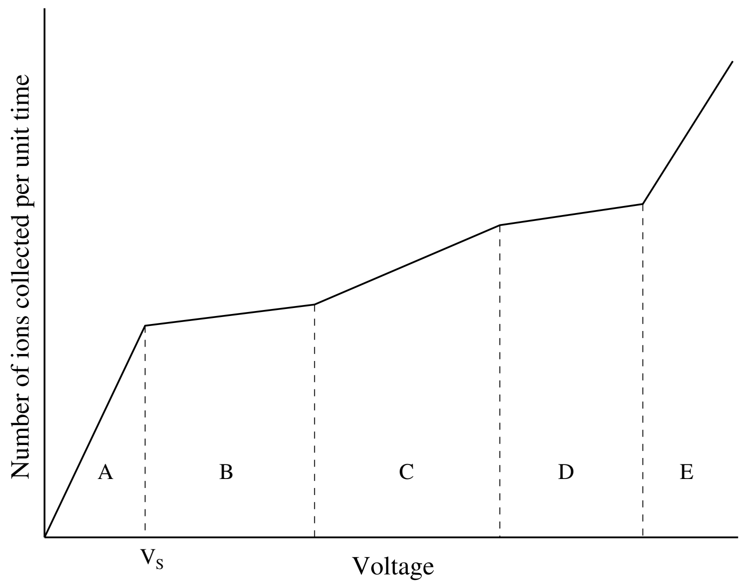

Figure 2.9: The voltage dependence of charge collection in a gas-filled detector. Region A is known as the recombination region. Region B is the ionization chamber or saturation region. Region C is the proportional counter region. Region D is the Geiger-Müller plateau and region E is the continuous discharge region.

Owing to the small electrical signal produced by a radiation event, ionization chambers are seldom used to count single radiation events. Rather, they are typically used to record the total amount of charge produced by a beam of radiation.

Proportional Counters and Neutron Detectors

For applied voltage beyond the ionization chamber region, a gas-filled detector enters the *proportional counter* region (C), in which the accelerated charges have sufficient kinetic energy to induce further ionizations through collision interactions. The output electrical signal is directly proportional to the energy deposited by the primary radiation and primary particle identification is possible.

In radiation protection, proportional counters are frequently encountered as neutron detectors. Since primary particle identification is possible, the photon background can easily be discriminated against. The slow neutron signal (from indirect neutron ionization) is enhanced by coating the chamber wall with a boron compound, or by filling the detector volume with BF_3 gas. Fast neutrons may be moderated by surrounding the detector with a moderator of hydrogenous material.

Geiger-Müller Detectors

At high voltages, gas-filled detectors operate in the *Geiger-Müller* (GM) region (D). In this plateau region, accelerated electrons excite gas molecules and produce UV radiation. The UV radiation, in turn, induces further ionization such that an avalanche of electron-ion pairs propagates through the gas volume. The output electrical pulse is very strong but is independent of the type or energy of the primary radiation. Accordingly, GM detectors are very sensitive and can detect all forms of ionizing radiation. They are commonly used as survey meters for radiation protection purposes.

Despite their excellent sensitivity, GM detectors have several disadvantages for surveying radiation therapy installations. They are unable to identify particle type since all radiations produce the same signal, and they suffer from saturation when measuring high dose-rate radiation. In the pulsed radiation field of a linear accelerator, the instantaneous dose rate may be extremely high, even if the time-averaged dose rate is considered "normal". This property of linear accelerator beams means that GM detectors are unsuitable for accurate measurements at radiation therapy facilities.

2.9.2 Themoluminescent Dosimeters

TLDs are radiation detectors that are based on the property of thermoluminescence. A thermoluminescent material (often referred to as phosphor) is a crystal with an energy-level diagram similar to that shown in Figure 2.10.

Phenomenologically, a thermoluminescent material may be modelled as comprising valence and conduction bands separated by an energy gap, with traps (storage traps and recombination centers) found within the gap. Traps can hold either electrons or positive holes and are generally caused by crystal impurities.

Before irradiation, the traps are empty, i.e., the electron traps are free of electrons and the hole traps contain electrons but no holes. When radiation passes through the crystal, it may excite an electron to the conduction band, from the valence band or from an empty hole trap. A hole is thus left behind in either the valence band or the hole trap. Similarly, a hole may be excited from the conduction band or an electron trap. The system may return to thermal equilibrium via three possible routes: (1) free charge carriers recombine, (2) a free charge carrier recombines with a trapped charge carrier of the opposite sign in a recombination center, with the emission of optical fluorescence, or (3) a free charge carrier becomes trapped in a storage trap and is only released on heating the crystal. When provided with sufficient energy to escape its trap, a charge carrier may move within the valence or conduction band (as appropriate for its charge) until it encounters a recombination trap into which it falls with emission of a visual or ultraviolet (thermoluminescent) photon. Radiation exposure, controlled heating and light measurement form the process through which TLDs are used to measure radiation.

TLDs are integrating-only dosimeters, in that they cannot provide instantaneous dose measurements. However, they offer good sensitivity and a high degree of accuracy in pulsed radiation fields. TLDs are commonly used as personal dosimeter badges, worn by radiation workers. In Canada, a national TLD-reading service is provided by Health Canada. Two important disadvantages of TLDs, is that they are unreliable in low-dose environments due to the

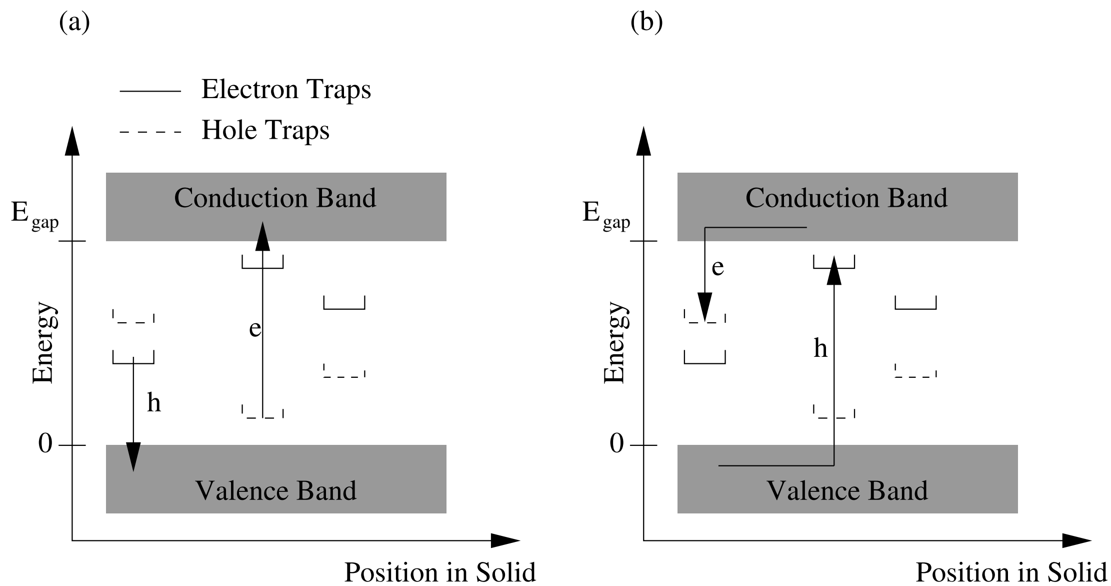

Figure 2.10: Energy-level diagram for a thermoluminescent material, showing electron and hole traps contained within the energy gap between the valence and conduction bands. (a) When irradiated, an electron may be excited from the valence band or a hole trap to the conduction band. Likewise, a hole may be excited from the conduction band or from an electron trap to the valence band. (b) When heated sufficiently, a trapped electron may gain enough energy to escape its trap. It may then move within the conduction band until it encounters a hole trap where it will combine with a hole and emit a visual or UV photon. Likewise, a trapped hole may escape to the valence band and move until it encounters an electron trap.

faint light signal produced and they can only be read once. The threshold for dose reporting by Health Canada is 0.1 mSv.

2.10 Production of Therapeutic Radiation Beams

Megavoltage therapeutic photon and electron beams are typically produced using linear accelerators. To produce an X-ray beam, a linear accelerator accelerates electrons toward a target whereupon bremsstrahlung X-ray photons and heat are produced. To produce an electron beam, the target is removed. As shown in Figure 2.11, there are several major components to a therapeutic linear accelerator: the gantry, the gantry stand and support, the head, the patient couch and the control console.

Depending on the type of linear accelerator involved, the radiation beam may be formed in the gantry stand or within the gantry itself (as is the case in Figure 2.11). Electrons are produced by means of thermionic emission and acceleration off a heated cathode within a device known as an *electron gun*. From the electron gun, the electrons drift into an accelerating RF waveguide. Within the waveguide they are accelerated to MeV energies as a result of energy transfer to them from the high-power RF field. The beam transport system controls delivery of the energetic pulsed electron beam from the waveguide to the target (for an X-ray beam) or to a scattering foil (for an electron beam). The purpose of the scattering foil is to spread out the otherwise narrow electron beam. Before reaching the patient, the beam is shaped within the head of the unit using collimating jaws made of high-Z material or using a computer-controlled multileaf collimator (MLC). Additional details regarding the geometry of radiation therapy treatment rooms is provided in section 3.2.

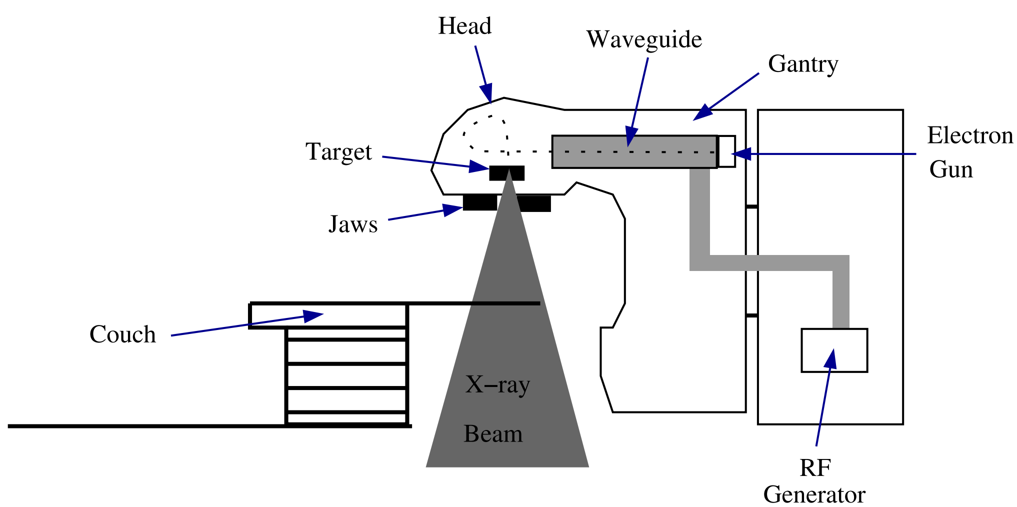

Figure 2.11: The main components of a linear accelerator used to produce megavoltage therapeutic photon and electron beams.

CHAPTER 3
Shielding Design

Internationally accepted guidelines for the design of structural shielding for radiation therapy installations are laid out in the National Council for Radiation Protection report number 151 (NCRP, 2005) and in the Institute of Physics and Engineering in Medicine (IPEM) report number 75 (IPEM, 1997), herein referred to as just NCRP 151 and IPEM 75, respectively. These reports detail the calculations involved in determining the barrier thickness needed to shield an individual from a source of radiation such that his/her effective doses are kept well below the appropriate maximum permissible values. They also provide general recommendations for the design of shielding around radiation therapy installations. A third report, the IAEA Safety Reports Series (SRS) No. 47. (IAEA, 2006), draws upon both NCRP 151 and IPEM 75 and is available free of charge on the IAEA website[1] .

This chapter describes the calculation methodology of the NCRP report, currently the standard shielding design document used for radiation therapy facilities in North America. This report, along with the NCRP report number 49, was used in the design calculations for the Radiation Oncology department at the Montreal General Hospital.

3.1 Equivalent and Effective Doses

The NCRP 151 authors use equivalent dose H as the single dose quantity of interest in all shielding calculations. They do so, despite the fact that

[1] http://www-pub.iaea.org/MTCD/publications/PDF/Pub1223_web.pdf

the ICRP and NCRP dose limit recommendations and the legal maxima prescribed by regulatory bodies, including the CNSC, are for both equivalent dose and effective dose. The reason to use equivalent dose alone is a matter of practicality—it is simply unfeasible to estimate effective dose values without exact prior knowledge of quantities such as the position, size and posture of the person who is exposed.

3.2 Treatment Room Geometry and Sources of Radiation

NCRP 151 considers megavoltage photon as well as electron beams used for radiation therapy. The applicable energy range varies from 1.25 MV to 24 MV. At these energies, linacs or cobalt-60 teletherapy units are employed and the radiation source is usually incorporated into a gantry that rotates in a single plane around the patient, the size of the radiation beam being controlled by the jaws or the multi-leaf collimator of the machine. The horizontal axis of rotation is referred to as the isocenter axis. The isocenter itself is the volume defined by the intersection of the isocenter axis and the axes of rotation of both the patient couch and the collimator of the radiation unit, and is typically close to the center of the treatment room. Figure 3.1 presents schematics of a typical radiation therapy treatment room, showing the position of the isocenter and the layout of the walls, ceiling and door.

Two types of radiation reach the walls of the room and must be accounted for in shielding design calculations: (1) primary beam (either attenuated through the patient or unattenuated) and (b) secondary radiation arising from leakage through the shielded head of the radiation generator and from scattered radiation produced by the interaction of the primary beam within the patient. Figure 3.2 is an illustration of the radiation beams of interest, together with the primary and secondary barriers used to shield them. Since the energy of the primary and secondary beams differ significantly, they must be

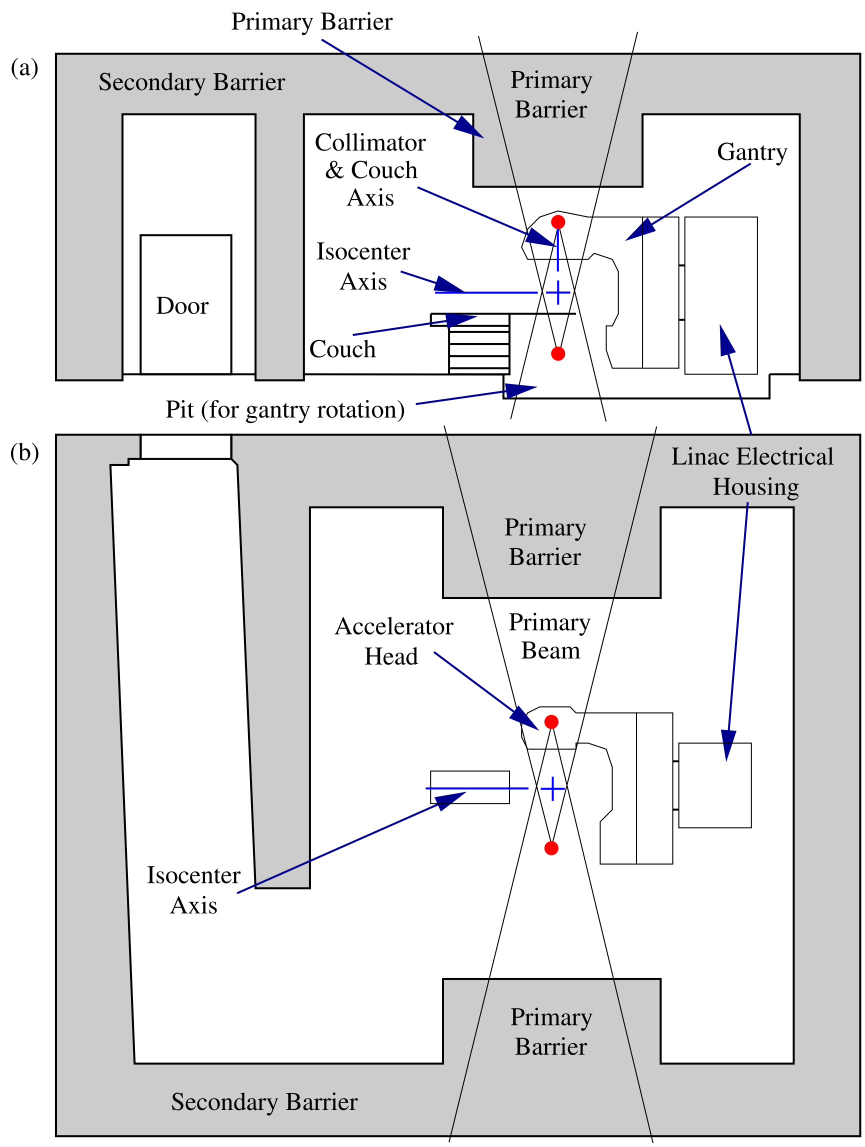

Figure 3.1: Schematics showing the geometry of a typical radiation therapy treatment room. (a) Front elevation view. (b) Plan view. The location of the isocenter is shown by a blue cross and the source positions for beam directions perpendicular to the viewing angle are marked by red dots.

considered independently and require separate shielding design calculations. The primary beam is a true beam in the sense that it is collimated in the direction of the isocenter, and thus "beamed" onto the wall, whereas the secondary radiation may travel in all directions and is usually assumed to originate at the isocenter[2] .

At high energies, above ~10 MV, two additional sources of secondary radiation must be considered; photoneutrons produced by photonuclear interactions within the machine head and within the patient, and subsequent gamma rays produced by neutron-capture interactions. Since neutrons scatter freely, they, and the capture gamma rays they produce, are also considered as multidirectional beams of secondary radiation emanating from the isocenter.

In addition to appropriate primary and secondary barriers, a treatment room must incorporate a shielded door for access, as shown in Figure 3.2. At low energies the door design is straightforward since only photons are involved. Above 10 MV, however, the presence of photoneutrons complicates matters considerably. A direct shielded neutron door (i.e., a door directly exposed to the secondary neutron beam) is often so large and heavy that it is impractical. Additional secondary barrier shielding to attenuate the secondary radiation before it reaches the door is required. A "maze" wall, forming a corridor from the door to the far wall of the room, is the solution. The treatment room depicted in Figures 3.1 and 3.2 incorporates a maze.

[2] Scatter radiation is actually produced from all points at which the primary beam encounters matter. Nevertheless, the assumption that it originates, on average, at the isocenter is valid when all gantry angles used in patient treatments are considered. It is also assumed that scatter by air molecules is negligible

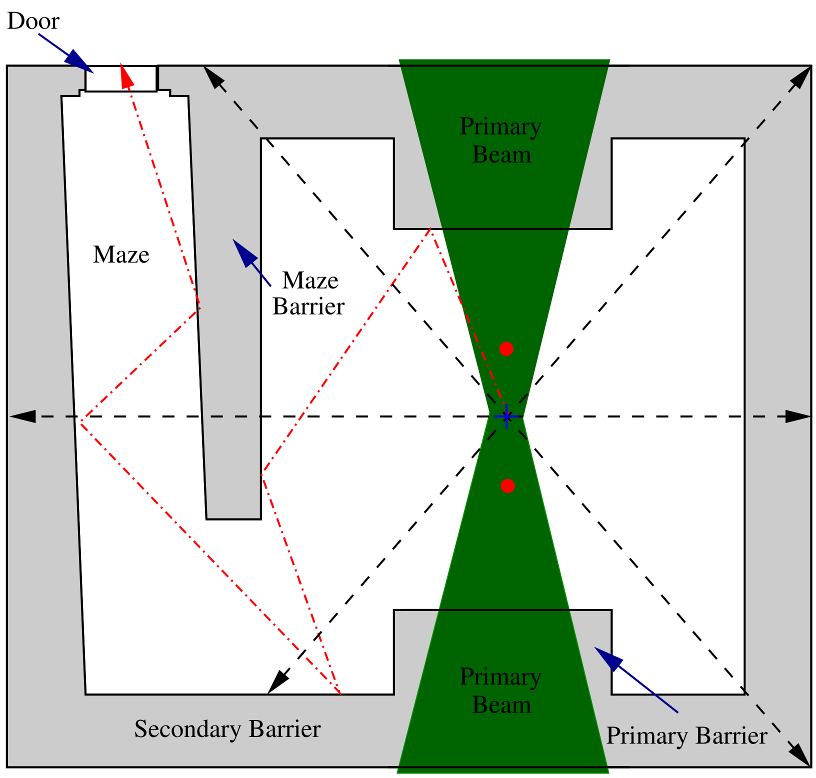

Figure 3.2: The primary (shaded green) and secondary (lines) radiation beams produced inside a radiation therapy room and the barriers used to provide shielding against them. Several secondary beams are shown—the black dashed line represents leakage and scatter, the dot-dashed line represents photoneutrons. As described in the text, all appear to emanate from the isocenter when all gantry angles are accounted for. The location of the isocenter is shown by a blue cross and the source locations for 180° gantry rotations are marked by red dots.

3.3 Shielding Materials

The shielding properties of a number of materials are detailed in chapter 4 of NCRP 151. Table 3.1 provides a summary. A comparison of materials used for photon shielding in megavoltage radiation therapy is quite straightforward since only a density comparison is required. This is due to the dominance of the Compton effect at megavoltage energies (see Figure 2.2) and the Z-independence of the Compton effect (see Table 2.1). However, with regard to shielding radiation from linear accelerators that accelerate electrons to energies above 10 MV, the ability of an attenuating material to absorb or moderate neutrons is an important additional consideration. High-Z materials, such as lead and steel are nearly transparent to fast neutrons, although they do moderate their energies. Materials with high hydrogen content (e.g., concrete) or borated materials (such as borated-polyethylene) are the best neutron absorbers.

3.4 Overview of Shielding Calculations

The purpose of any radiation shielding calculation is to determine the thickness of a barrier needed to reduce the radiation dose received at a point of interest (POI) at one side of the barrier, due to a radiation source at the other side, to a desired level. In NCRP 151, the desired radiation level is called the "design goal" P. Its value is equal to the regulatory dose limit modulated by an appropriate ALARA factor (see section 1.6.7). Figure 3.3 graphically depicts the geometry, distances and quantities involved in a shielding calculation.

In the NCRP 151 calculation, the barrier attenuation factor B, by which the barrier must attenuate the dose produced inside the room to the desired level outside, is determined. The number of tenth value layers (TVLs) of barrier material required to provide B is then calculated. Finally, the barrier

Material	Density (g cm^{-3})	Hydrogen Content $\times 10^{22}$ atoms cm^{-3}	Primary Barrier Thickness (m)	Relative Cost	Advantages	Disadvantages
Ordinary Concrete	2.35	0.8 to 2.4	2.5	$$	Easy to pour/configure, relatively inexpensive, easily available, good X-ray shielding, good neutron shielding, structurally strong	Large footprint in terms of barrier thickness
HD Concrete	> 2.35	0.8 to 2.4	1.4	$$$$	Small footprint compared to ordinary concrete	Handling difficulties. Primary barrier adequate for photons not necessarily adequate for neutrons
Lead	11.35	None	0.5	$$$	Thin barriers	Lead is malleable and needs to be supported against its own weight. Toxic. Nearly transparent to fast neutrons
Steel	7.8	None	0.8	$$	Relatively thin barriers, strong, less expensive than lead	Nearly transparent to fast neutrons
Polyethylene	$\sim$1.04	8.0	5.7	$$$	Useful for shielding neutrons. Particularly useful as borated polyethylene, with 5 % Boron by weight	
Paraffin	$\sim$1.04	8.0	5.7	$$$	Useful for shielding neutrons	
Earth	$\sim$1.5	Similar to concrete	3.9	Cheap	Low cost, easy to install	Density may be difficult to quantify
Wood	$\sim$0.65	6 % by density	9.0	Cheap	Low cost, easy to fabricate	Large footprint in terms of barrier thickness

Table 3.1: Summary of the properties of the shielding materials encountered in NCRP 151. Primary barrier thicknesses equivalent to 2.5 m of ordinary concrete are provided.

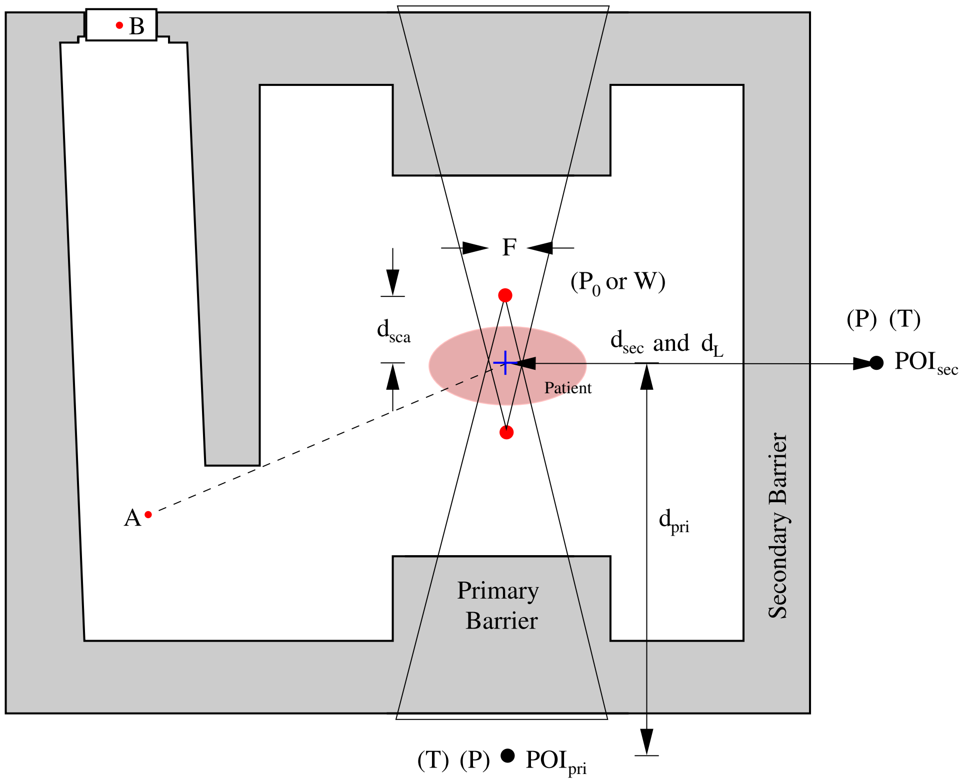

Figure 3.3: The geometry, distances and quantities involved in shielding calculations for primary and secondary barriers. Quantities are shown in parenthesis. P_0 and W correspond to the workload of the machine in the treatment room, with W in the same units as the design goal P. T is the occupancy factor of the room containing the POI. The letters A and B denote the positions of the inside and outside maze entrances respectively, of importance for neutron shielding considerations, as described in section 3.7.2. The dashed line shows how position A is determined.

thickness is determined using the number of TVLs and appropriate TVL tables that are provided in the appendix of NCRP 151.

3.4.1 Determination of the Barrier Attenuation Factor B

The steps involved in the calculation of a barrier attenuation factor B are described here. The overall steps are the same for both the primary and secondary barriers but with important differences in the details, as described in section 3.6 below.

Step 1: To ensure compatibility of the units used in the shielding calculation, it is first necessary to convert the unit of dose rate used to describe the radiation source (linac or teletherapy machine) to the unit used to describe the design goal P. Typically, gray per year (Gy/yr) is the unit of choice for P, since it corresponds to the regulatory limits.

The workload W of a radiation therapy machine is a measure of the average dose it produces in water at its isocenter over a specified period of time. As such, the known or projected annual workload (in Gy/yr) is the quantity most appropriate for shielding calculations. A realistic and accurate estimate of W is vital for proper shielding design. It is a quantity that must be estimated by the designer from patient treatment projections. Unlike most of the other parameters encountered in a shielding calculation, W is specific to the treatment room involved and its value is neither prescribed nor recommended by the NCRP or by the regulatory authorities.

Step 2: A highly conservative estimate for B may be calculated by scaling W (i.e., the dose rate within the room) to the desired dose rate at the POI outside the room P, with the inverse-square law accounted for by a d^2 factor, where d is the distance from the source to the POI, as shown in Figure 3.3):

$$B = \frac{Pd^2}{W} \tag{3.1}$$

Step 3: To determine a more realistic value for B (i.e., one that does not grossly over-shield), the room occupancy T at the POI and the usage U of the barrier must be considered. The resulting expression for B is thus:

$$B = \frac{Pd^2}{WUT} \tag{3.2}$$

The occupancy factor T is a scale factor that accounts for the true amount of time during which the room containing the POI is actually occupied over

Location	Occupancy Factor (T)
Full occupancy areas (areas occupied full-time by an individual), e.g., administrative or clerical offices; treatment planning areas, treatment control rooms, nurse stations, receptionist areas, attended waiting rooms, occupied space in nearby building	1
Adjacent treatment room, patient examination room adjacent to shielded vault	1/2
Corridors, employee lounges, staff rest rooms	1/5
Treatment vault doors	1/8
Public toilets, unattended vending rooms, storage areas, outdoor areas with seating, unattended waiting rooms, patient holding areas, attics, janitors' closets	1/20
Outdoor areas with only transient pedestrian or vehicular traffic, unattended parking lots, vehicular drop off areas (unattended), stairways, unattended elevators	1/40

Table 3.2: NCRP 151 suggested occupancy factors.

the calculation period. For example, if the POI is the control room, it can be assumed to have full occupancy ($T = 1$), since the radiation therapist is always at the console while the beam is on. If, however, the POI is in an adjacent room that is seldom occupied, it should have an occupancy factor less than 1.0. The list of room occupancy factors recommended by the NCRP are listed in Table 3.2.

The use factor U accounts for the fact that the radiation beam may be directed at the target volume within the patient from multiple directions by rotating the gantry. If the primary beam were only to strike the single primary barrier between the source and the POI, that barrier's use factor would be 1.0. However, this is never the case, and the use factors of the four walls (two vertical walls plus the ceiling and floor) typically average out to 0.25 each. In certain situations, for example in treatment rooms used heavily for TBI or TSEI treatments, the use factor of interest may be more or less than 0.25. The use factor is always 1.0 (and so is ignored) in secondary barrier calculations, since secondary radiation beams are assumed to be multidirectional.

At a first glance, equation 3.2 results in a value for B with units of m^2. However, the authors of NCRP 151 get around this by referencing all distances in the report to a distance of 1 m. Hence, the d^2 factor is divided by 1 m^2 and the resulting value for B is unitless.

3.4.2 Determination of the Number of TVLs and Barrier Thickness

With the barrier attenuation factor known, the corresponding number of TVLs n_{TVL} of the radiation beam in the barrier material is simply calculated using:

$$n_{\mathrm{TVL}} = log_{10}\left(\frac{1}{B}\right) \tag{3.3}$$

NCRP 151 recommends that, for primary barrier calculations, the first TVL TVL_1 should be considered separate to the remaining "equivalent" TVLs TVL_{e}. The authors reason that the hardening of the beam as it traverses the first TVL results in longer subsequent TVLs.

Finally, the required barrier thickness t_{barrier} is calculated as

$$t_{\mathrm{barrier}} = TVL_1 + (n-1)TVL_{\mathrm{e}} \tag{3.4}$$

NCRP 151 provides TVL thickness tables for ordinary concrete, lead and steel.

3.5 Primary Barrier Calculation

All the factors discussed above considered, the barrier attenuation factor for the primary beam is given by the equation:

$$B_{\mathrm{pri}} = \frac{Pd_{\mathrm{pri}}^2}{WUT} \tag{3.5}$$

where a use factor less than 1.0 is typically employed. In calculating the primary barrier thickness, NCRP 151 makes the conservative assumption that the primary beam is unattenuated in traversing the patient (this is not the case in IPEM 75). Accordingly, when undertaking a post-construction radiation survey, a phantom should not be used in evaluating the primary barrier, if survey results are to be compared with NCRP 151 predictions.

3.6 Secondary Barrier Calculation

The secondary barrier must shield against both the leakage and scatter radiations. As described in section 2.2.3, at megavoltage energies the dominant photon interaction is the Compton effect. In the Compton interaction, the photon is not absorbed, rather it is scattered at an angle and with reduced energy. Both the leakage and scatter radiations undergo Compton scattering. The leakage beam scatters multiple times, and thus looses significant energy, while traversing the dense material (typically lead) in the head of the radiation generator. The scatter radiation, by definition, is scattered at least once before reaching the secondary barrier.

Two main sources of scatter radiation are possible: (1) scatter radiation produced by scattering of the primary beam within the patient, and (2) scatter radiation produced by scattering of the primary and patient scatter radiations with the walls and fixtures of the treatment room. A secondary barrier with thickness adequate to attenuate: (1) will generally be sufficient for (2), since multiple scattering interactions reduce photon energy and penetrability significantly.

Barrier thicknesses are calculated for the leakage and patient-scatter beams independently due to the difference in energy between them. Leakage radiation, having undergone multiple scattering within the head of the treatment machine, is typically of a much lower energy than the patient-scatter radiation, which is scattered less often before reaching the walls.

As mentioned previously, a use factor of unity is used in secondary barrier calculations, since the secondary radiations are emitted in all directions.

Shielding Calculation for Leakage Radiation

IEC (International Electrotechnical Commission) regulations stipulate that the leakage from the head of a radiation-therapy unit must not exceed an average of 0.1 % and a maximum of 0.2 % of the primary beam over a 2 m radius measured from the beam central axis in the plane of the patient (IEC Publication 601-2-1, 1981). NCRP 151 takes a conservative approach and simply assumes that the leakage is equal to 0.1 % of the primary beam, even though the authors point out that manufacturers generally shield their machines to better than 0.1 %. The barrier attenuation factor for the leakage beam alone is thus given by the equation:

$$B_{\mathrm{L}} = \frac{P d_{\mathrm{L}}^2}{10^{-3} W_{\mathrm{L}} T}, \tag{3.6}$$

where d_{L} corresponds to the distance from the POI to the source of the leakage, which, as shown in Figure 3.3, generally averages to the isocenter. The leakage workload W_{L} may be assumed to be equal to the normal workload W except for clinical practice that involves a large component of IMRT—in IMRT treatments, small field sizes are used and more “beam-on” time (larger leakage workload) is required to produce the same absorbed dose at the isocenter. Leakage-specific TVL tables are provided in the appendix of NCRP 151.

Shielding Calculation for Patient Scattered Radiation

The barrier attenuation equation used for patient scattered radiation is

$$B_{\mathrm{ps}} = \frac{P}{\alpha W T} d_{\mathrm{sca}}^2 d_{\mathrm{sec}}^2 \frac{400}{F}, \tag{3.7}$$

where (with reference to Figure 3.3):

- α is the scatter fraction or the fraction of the primary beam absorbed dose that scatters at a particular angle. Scatter fraction tables are provided in the appendix of NCRP 151.
- d_{sca} is the distance from the primary radiation source to the scattering material (the patient). Usually taken as the SAD of the machine.
- d_{sec} is the distance from the scattering point to the POI.
- F is the treatment field area (in cm^2) at the isocenter. The factor of 400 accounts for the fact that the scatter fractions provided in NCRP 151 are normalized to those measured for a 20 cm $\times$ 20 cm field size.

The scattering angle does not directly enter into the barrier attenuation equation but is considered instead in the scatter fraction lookup-table.

The Two Source Rule

Using the calculated barrier attenuation factors B_{L} and B_{ps}, for leakage and patient-scatter, respectively, the final required thickness of the shielding material can be determined. The barrier thicknesses required for each are compared as though there were two separate sources in the treatment room. If they are about the same (less than 1 TVL difference), then their combined dose at the POI should be about double their individual values. A half value layer (HVL) is, therefore, added to the greater of the two to reduce the combined dose by one half. If the thicknesses differ significantly (by 1 TVL or more), the larger thickness will provide adequate shielding for both.

3.7 Maze and Door Calculations

As mentioned previously, the door of a treatment room controls access to the room while simultaneously providing shielding. One could employ a direct shielded door made from lead or steel and simply use the NCRP secondary barrier calculation methodology to determine its thickness. While adequate at low energies, such a direct shielded door would become prohibitively impractical at high energies where the secondary radiation is more penetrating. Above 10 MV, photoneutrons and neutron-capture gamma rays are an additional hazard that require further shielding. The solution is a maze barrier to attenuate the secondary radiation before it reaches the door. Figure 3.2 shows the geometry of a maze wall.

NCRP 151 provides a recipe to calculate the reduced secondary dose at the treatment room door when a maze is used. With regard to photon dose, the calculation method is the same regardless of energy; the energy being accounted for in the tabulated data provided. At high energies, however, the photoneutron and neutron-capture gamma-ray dose must be added to the photon dose.

3.7.1 Photon Dose

In calculating the photon dose (i.e., not including neutron-capture gamma rays) at a treatment room door at the end of a maze, four sources of secondary radiation are considered, as shown in Figure 3.4:

1. Scatter of the primary beam off the primary barrier to the maze outer wall and a second scatter off the maze outer wall to the door, H_{S}. Black dashed line in Figure 3.4.
2. Scatter of the leakage beam off the wall at the end of the maze to the door, H_{LS}. Red dash-dotted line in Figure 3.4.
3. Scatter of the patient-scattered beam off the wall at the end of the maze to the door, H_{ps}. Green dash-double-dotted line in Figure 3.4.
4. Direct transmission of leakage radiation through the inner maze wall to the door, H_{LT}. Blue dotted line in Figure 3.4.

The NCRP 151 report authors caution that their method for estimating the door dose should be restricted to rooms where the maze height to width ratio

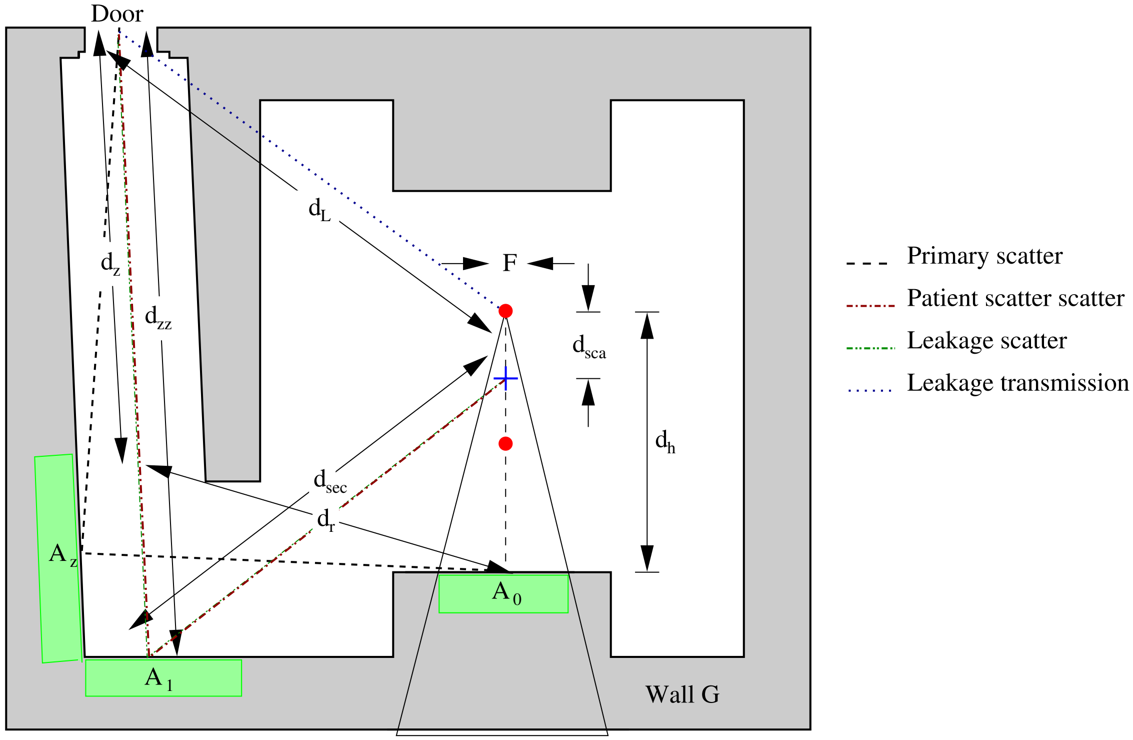

Figure 3.4: The geometry, distances and quantities involved in calculating the dose at the door for a low-energy (< 10 MV) radiation therapy treatment room. The location of the isocenter is shown by a blue cross and the source locations for 180° gantry rotations are marked by red dots. Radiation trajectories are shown using dashed and dotted lines.

is between 1 and 2, and where the ratio of the maze length to the mean of the maze width and height is between 2 and 6.

Each dose component is calculated separately for the primary beam striking a single wall (wall G, corresponding to the wall opposite the door and at the end of the maze corridor, as shown in Figure 3.4) and then combined to give the expected total secondary radiation at the treatment room door, for the single wall. All four walls (right, left, ceiling and floor) are then accounted for, using an experimentally-determined combination factor of 2.64 (as opposed to simply multiplying by 4). Knowing the dose at the inside of the door, its barrier attenuation factor and thickness can be calculated for the appropriate design goal as for the primary and secondary barrier calculations.

Primary Beam Scatter Component

The primary beam must scatter twice in order to reach the treatment room door. The first scatter is off the primary barrier, the second is off the outer wall of the maze, Figure 3.4. Thus, two scatter fractions (a_z off the primary barrier and a_0 off the outer maze wall) and three inverse-square law factors (source to primary barrier d_h, primary barrier to center of maze d_r, and maze center to door d_z) are needed[3] . The machine's workload and the primary beam's usage onto wall G are also accounted for. The equation for the equivalent dose at the door due to primary beam scatter is thus

$$H_S = \frac{\alpha_0 A_0 \alpha_z A_z W U_G}{d_h^2 d_r^2 d_z^2}, \tag{3.8}$$

where

- W is the workload of the machine in units corresponding with those of the design goal.
- U_G is the use factor for wall G.
- A_0 is the area of the primary barrier struck by the primary beam.
- A_z is the area of the outer maze wall struck by the scattered primary beam.

Head Leakage Scatter Component

Head leakage radiation is emitted in all directions, with the source position averaging to the isocenter when all gantry angles are considered. Given the geometrical restrictions imposed by the inner maze wall, only area A_1 of wall G can provide a single scattering route for the leakage beam to treatment room

[3] Although the inverse-square law is really only valid for a point source, it is used empirically for wall-scattered radiation in NCRP 151, presumably for its usefulness in simplifying the calculations

door, as shown in Figure 3.4. Multiple scattering routes need not be considered since the final photon energy would be sufficiently low to be neglected. As such, a single scatter fraction α_z and two inverse-square law factors (source to scattering region of wall G d_{sec} and wall G to door d_{zz}) are required. The equation for the contribution of the head leakage scatter to the dose at the treatment room door is thus

$$H_{LS} = \frac{L_f W_L U_G \alpha_1 A_1}{d_{sec}^2 d_{zz}^2} \tag{3.9}$$

where

- L_f is the leakage radiation ratio at 1 m from the source (taken as 0.1 %) as described in section 3.6.
- W_L is the leakage workload of the machine in units corresponding with those of the design goal.
- U_G is the use factor for wall G.
- A_1 is the area of wall G that may directly scatter radiation to the door of the treatment room.

Scatter fraction tables for beams with various energies, incidence angles, and scattering angles are provided in the appendix of NCRP 151 for concrete, iron and lead. A note in the text (page 37) suggests using an effective leakage energy of 1.4 MeV for a 6 MV beam and 1.5 MeV for a 10 MV beam. However, in the example calculation provided in the document, the authors actually use the maximum beam energy in determining the scatter fraction for head leakage. The present effort followed the methodology of the example calculation.

Scattered Patient Scatter Component

Patient scatter, like head leakage, emanates on average from the isocenter and thus is restricted by the maze wall to the region A_1 of wall G, if it is to reach the door in a single scatter. The single wall scatter fraction, α_1 and the two inverse-square law factors, d_{sec} and d_{zz}, are thus employed. A second scatter factor, $a(\theta)$, and a third inverse-square law factor, d_{sca} (= SAD) account for scatter of the primary beam at the isocenter within the patient. Field size F has an effect on the amount of patient scatter and must also be accounted for. As for the secondary barrier calculation, the field size is divided by 400 since the scatter fractions were normalized to measurements made for a 20 cm $\times$ 20 cm field. All considerations included, the equation for the dose at the door due to scatter of the patent-scattered radiation is

$$H_{\text{ps}} = \frac{a(\theta) W U_{\text{G}} \left(\frac{F}{400}\right) \alpha_1 A_1}{d_{\text{sca}}^2 d_{\text{sec}}^2 d_{\text{zz}}^2}, \tag{3.10}$$

where

- θ is the angle at which the primary beam is scattered by the patient in order to reach the area A_1 of wall G.

Transmitted Leakage Radiation Component

Both leakage and scatter radiation can, in principle, pass directly but attenuated through the inner maze wall. In practise, it is only necessary to consider the leakage radiation, since photons that have been Compton-scattered at a large angle retain very little of their original energies.

The contribution to the door dose by leakage radiation transmitted through the inner maze wall is calculated by first determining B for the leakage radiation through the maze wall and then accounting for the leakage radiation ratio, the leakage workload and inverse-square law. The appropriate equation is

$$H_{\text{LT}} = \frac{L_{\text{f}} W_{\text{L}} U_{\text{G}}(=1) B}{d_{\text{L}}^2} \tag{3.11}$$

where

- d_L is the distance from the isocenter to the door through the inner maze wall.
- L_f is the leakage radiation ratio at 1 m from the source (taken as 0.1 %) as described in section 3.6.

It is not clear why the usage of wall G is included in the calculation of the dose at the door due to leakage radiation passing through the inner maze wall. It is presumably a typographical error in NCRP 151 and is, as such, set to unity for all calculations in the present work.

Combination of All Components

The equivalent dose at the maze door for all four radiation components, with the beam directed at wall G, is given by their sum, accounting for the fraction of the primary beam which is actually transmitted through the patient[4] :

$$H_G = fH_S + H_{LS} = H_{ps} + H_{LT} \tag{3.12}$$

where f is the fraction of the primary beam transmitted through the patient ($f = 0.25$ for 6-10 MV X rays for a field size of 40 cm $\times$ 40 cm).

Accounting for the four cardinal directions to which the primary beam may point (ceiling, floor, left, right) the total equivalent dose at the maze door is given by:

$$H_{Tot} = 2.64H_G \tag{3.13}$$

The factor of 2.64 was experimentally determined and is less than four since each beam direction contributes differently to the final dose at the door, with the wall G direction contributing the most.

[4] It is interesting that the NCRP chose to consider the attenuation of the primary beam by the patient in their door and maze calculations, considering that they chose not to do so in the primary barrier calculation

3.7.2 Neutron Considerations for High-Energy Beams

As described in section 2.2.5, at energies above $\sim$10 MeV the photonuclear interaction is energetically feasible and thus presents a shielding challenge for high-energy radiation therapy installations. Two types of radiation exposure to patients and medical personnel must be considered and are dealt with in NCRP 151: (1) "beam-off" exposure within the treatment room due to radiation from activated materials, and (2) "beam-on" neutron and neutron-capture gamma-ray radiation produced during treatments.

For beam-off exposure resulting from activated materials, NCRP 151 provides a list of the principal radionuclides encountered and a corresponding list of predicted equivalent doses resulting from routine exposure to them. The NCRP 151 authors cite the work of Rawlinson et al. (2002), who found that equivalent dose rates within a treatment room are very close to background 48 hours following exposure with no appreciable long-term buildup of activity. They also point out that there is little in the way of shielding design that can decrease the exposure to personnel from activated materials. Simultaneous to the publication of NCRP 151, a thorough study of treatment room activation at the MGH was reported on by Wang et al. (2005).

NCRP 151 deals comprehensively with the much more significant beam-on exposure risk from neutrons and neutron-capture gamma rays. The appropriate shielding design considerations are dealt with in a dedicated section that describes the door and maze calculations for high-energy installations. The authors point out that primary and secondary barriers designed for high-energy photon fluxes should be sufficient to deal with neutron and neutron-capture gamma-ray fluxes, owing to the thicknesses involved. For thin barriers such as the door, however, neutron-capture gamma rays and photoneutrons present an important hazard. In fact, according to McGinley and Huffman (2000), for treatment rooms with mazes of length (distance from A to B in Figure 3.3) greater than 2.5 m, the neutron-capture gamma-ray flux at the door exceeds the secondary photon flux such that the neutron-capture flux can be considered as the sole photon source in the door-design calculation.

The NCRP 151 calculation for the equivalent dose H_{cg} arising from neutron-capture gamma rays at the door follows the method of McGinley et al. (1995). It essentially entails a two-step calculation, whereby the neutron flux at the inner maze entrance (location A in Figure 3.3) is estimated and then used to determine the dose at the outer maze entrance (i.e., at the door). Suggested analytical techniques to estimate the neutron equivalent dose H_{n} at the door are provided, using either the original method of Kersey (1979) or a modified version thereof provided by Wu and McGinley (2003). The final equivalent dose H_{w} at the door location for high-energy treatment rooms is then the sum of the photon dose (as per the low-energy calculation detailed in section 3.7.1), the neutron-capture gamma-ray dose and the neutron dose):

$$H_{\text{w}} = H_{\text{Tot}} = H_{\text{cg}} + H_{\text{n}} \tag{3.14}$$

3.7.3 Door Design

The thickness of the door required for a radiation therapy room may be calculated once the dose at the door has been established. For low-energy accelerator rooms, the door typically comprises a lead barrier encased in steel for rigidity. The transmission factor for the lead is calculated by dividing the shielding design goal P for the area outside the door by the photon dose determined just inside it. The design goal may be modulated by the 1/8 occupancy factor, as per Table 3.2.

Doors used for high-energy accelerator rooms must shield against the photon dose together with the neutron and neutron-capture gamma-ray doses. A door comprising a sandwich of lead, borated-polyethylene (BPE) and lead, encased in steel is typically employed. The inner layer of lead serves to moderate fast neutrons from the treatment room by inelastic scattering, making the central layer of BPE more effective at thermalizing and absorbing them.[5] The outer layer of lead serves to attenuate the gamma rays that result from neutron capture by the boron. Once transmission factors have been established, both for lead and BPE, the required thicknesses of each may be determined from tables provided in the appendix of NCRP 151.

3.8 Instantaneous and Time Averaged Dose Rates

Any dose rate measurement necessarily involves some amount of averaging—an "instant" has duration, even if very small. In the IAEA SRS 47 report, the instantaneous dose rate (IDR) is defined as the direct reading of a survey meter that gives the dose per hour, averaged over a minute. The IDR is used but not defined in NCRP 151.

For continuous sources such cobalt-60 teletherapy units, the IDR is easy to visualize. Regardless of the duration of the measurement, the dose rate remains the same. For pulsed radiation sources such as linacs, however, the duty cycle of the machine somewhat complicates the IDR determination. Electrons are typically only accelerated within the waveguide for just 0.02 % of the beam-on time. The instantaneous dose rate, if measured during the true beam-on portion of the pulse, would be enormous. Averaging the dose rate

[5] Polyethylene (the polymer found in plastic bags) is hydrogen rich and serves as a good material for the moderation (slowing down) of fast neutrons to thermal energies through elastic scattering. Boron-10 is very effective at absorbing thermal neutrons through neutron capture.

over a minute, as per the IAEA SRS 47 report, is thus a convenient means of ensuring proper reporting of the IDR for a pulsed beam.

A similar duty-cycle argument may be applied to a workload that is averaged over a year or a week. It may not best represent the likely higher true dose rate measured over a shorter time period, such as a day or an hour. Indeed, averaging the dose rate over a long time period may be incompatible with the ALARA principle. The concept of the time-averaged dose rate (TADR) was introduced in NCRP 151 as a solution to time-averaging problems. The TADR is defined as the barrier-attenuated dose rate averaged over a specified time or period of operation. It takes into account the true workload over the time period and the usage of the barrier involved. Two time periods are considered in NCRP 151: the week and the hour.

3.9 Radiation Shielding Evaluation

Following installation of a new radiation therapy device, an evaluation of the adequacy of the treatment room shielding is necessary before routine operation may begin. The objective of the evaluation is to determine if the design goal has been achieved and to search for possible radiation leaks. Physical inspection of the shielding and a radiation survey behind all barriers are required.

The purpose of a physical inspection is to ensure that: (a) the shielding is constructed as designed and (b) no regions of potential radiation leakage (e.g., misplaced conduits) exist. An evaluation of the various interlocks, warning lights and signs that provide non-shielding protection is also required.

The radiation survey comprises comprehensive measurements of the radiation levels outside each barrier for all operating modes of the radiation generator. Each measured radiation level should be compared with the expected level determined from the shielding calculations used in the design.

In determining an expected radiation level, an inverse shielding calculation is essentially performed. The calculation begins with the known barrier thickness, from which the number of tenth value layers, and hence the expected attenuation factor, of the radiation beam in the shielding material may be calculated. Since the physical measurement is instantaneous, usage and occupancy factors of unity are used and the machine's workload is replaced by its instantaneous dose rate.

3.10 Additional Calculations and Recommendations in NCRP 151

In addition to the basic shielding calculations, NCRP 151 addresses various considerations that must be accounted for in several special situations, including Intensity Modulated Radiotherapy (IMRT), Tomotherapy, CyberKnife therapy, cobalt-60 teletherapy and intraoperative radiation therapy. Physical data are provided for a number of shielding materials and structural details of interest in construction of facilities are discussed. A large section of the document is devoted to a number of helpful example calculations.

CHAPTER 4
An Experimental Evaluation of the NCRP 151 Report

To evaluate the validity of the NCRP 151 formalism use was made of the radiation therapy treatment rooms in the Department of Radiation Oncology at the Montreal General Hospital (MGH). Several linear accelerators were investigated, operating in photon mode and using the available energies (6 MV and 18 MV). Geometrical parameters for the treatment rooms were determined from Computer Aided Design (CAD) plans of the department and verified through physical measurements. The NCRP 151 formalism, together with the geometrical data, was used to predict barrier-attenuated doses. Dose measurements were carried out using a variety of radiation measuring devices. Measured doses were compared with the NCRP 151 predictions. A detailed description of the predictions, the measurements, and the radiation therapy facilities at the MGH is provided in this chapter.

4.1 Radiation Therapy Facilities at the MGH

The MGH is a teaching hospital within the McGill University Health Centre (MUHC), a network of Montreal hospitals affiliated with McGill University. The MUHC provides a full range of cancer treatment services including radiation therapy.

The Department of Radiation Oncology is located on the fifth floor of the MGH building, one floor below the street-level entrance at 1650 Cedar Avenue, on the southern slope of the Mont Royal hill that gives the city of Montreal its name. The department has seven radiation therapy treatment rooms along the building's northwest side, under the drop-off driveway of the hospital and abutting the side of the adjacent Mont Royal hill. The basement location and hill adjacency provide natural rock shielding for the floors and northwest walls of the treatment rooms. Occupancy of the space above the treatment rooms is low by virtue of the transient vehicular and pedestrian traffic ($T = 1/40$, as per Table 3.2). Figure 4.1 presents an annotated CAD plan of the Radiation Oncology department, showing the treatment rooms and patient waiting areas. Six linear accelerator machines (five of which were manufactured by Varian Medical Systems, Palo Alto, California and the sixth by TomoTherapy, Madison, Wisconsin) a cobalt-60 teletherapy unit (manufactured by Atomic Energy of Canada, Limited) for TBI treatment, and a high dose rate (HDR) brachytherapy suite are available. The treatment rooms, machines, and associated treatment modalities are listed in Table 4.1.

CAD plans of the Radiation Oncology department, in DWG (drawing) format, were obtained from the technical services department of the MUHC. The *EveryDWG* file converter software, provided by the Open Design Alliance (www.opendwg.org), was used to convert the plans from DWG to DXF (Drawing Exchange Format) for reading using the *qCad* program developed by *RibbonSoft* for linux (www.qcad.org). The qCAD software provided convenient tools for the measurement of distances and angles within each treatment room. Figure 4.2 provides an example of a qCAD screenshot showing the distances and angles measured for the Clinac 21EX-A treatment room (D5 228) at the MGH. A photograph of the Clinac 21EX-A linear accelerator is shown in Figure 4.3

4.1.1 Occupancy and Workload Data

As mentioned in section 3.4, accurate information pertaining to the number and nature of people (both medical personnel and patients) passing through a radiation therapy department is vital for proper shielding design. At the MGH,

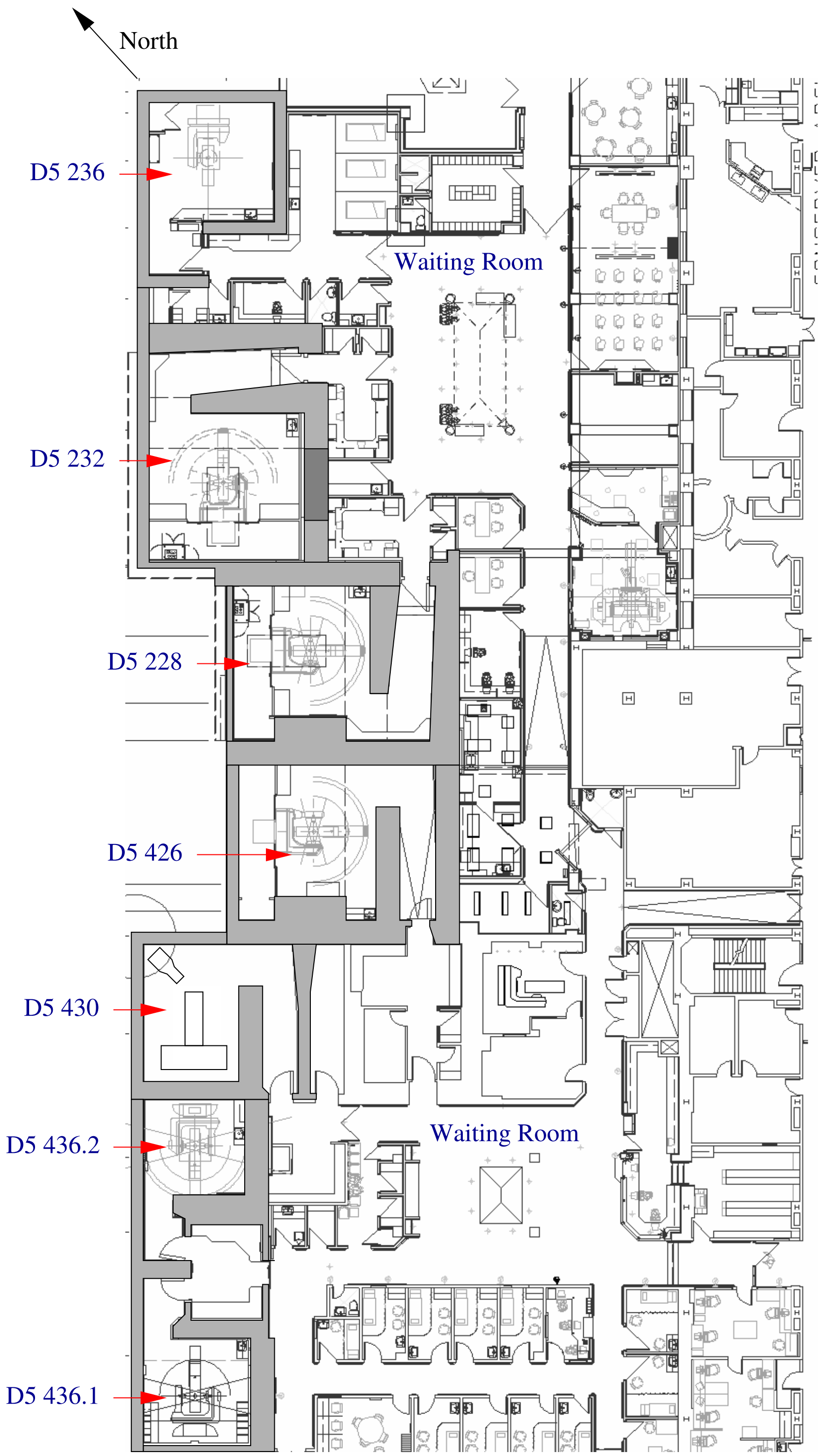

Figure 4.1: Annotated CAD plan of the Department of Radiation Oncology at the Montreal General Hospital. Room numbers are identified for cross-reference with Table 4.1. Patient waiting areas and radiation shielding barriers are highlighted.

Room	Maze	Machines	Mode	Energy	Treatment Techniques
D5 436.1	No	Varian Clinac 6EX-A	X rays	6 MV	3D RT, IMRT
D5 436.2	No	Varian Clinac 6EX-B	X rays	6 MV	3D RT, IMRT
D5 426	Yes	Varian Clinac 2300	X rays	6 MV	3D RT, IMRT, Stereotaxtic radiosurgery/radiotherapy
				18 MV	3D RT, Stereotaxtic radiosurgery/radiotherapy
			Electrons	6 MeV	
				9 MeV	
				12 MeV	
				15 MeV	
				18 MeV	
				22 MeV	
D5 228	Yes	Varian Clinac 21EX-A	X rays	6 MV	3D RT, IMRT
				18 MV	3D RT
			Electrons	4 MeV	
				6 MeV	TSEI treatments
				9 MeV	
				12 MeV	
				16 MeV	
D5 232	Yes	Varian Clinac 21EX-B	X rays	6 MV	3D RT, IMRT
				18 MV	3D RT
			Electrons	6 MeV	
				9 MeV	
				12 MeV	
				16 MeV	
				20 MeV	
D5 430	Yes	Tomotherapy	X rays	6 MV	Helical IMRT
		Cobalt-60 Teletherapy	γ rays	1.25 MeV	TBI treatments
D5 236	No	Ir-192 Afterloader unit	γ rays	0.4 MeV	HDR Brachytherapy

Table 4.1: List of radiation therapy treatment rooms, radiation generating machines and available treatment modalities in the Department of Radiation Oncology of the Montreal General Hospital.

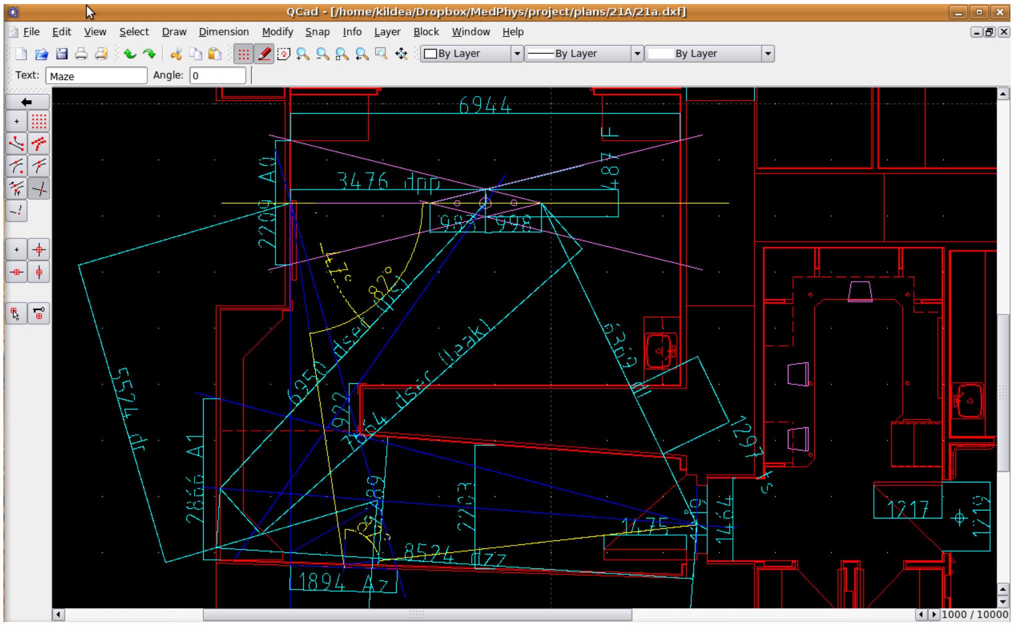

Figure 4.2: An example of a qCAD screenshot showing the distances and angles measured for the Clinac 21EX-A treatment room.

Figure 4.3: Photograph of the Clinac 21EX-A linear accelerator in room D5 228 of the Department of Radiation Oncology at the Montreal General Hospital. In the picture the gantry is rotated to 90° to face the wall G and a solid water phantom is positioned in the beam.

patient records are maintained by the ARIA Oncology Information System. ARIA is a comprehensive record-and-verify and Electronic Medical Records (EMR) database system provided by Varian Medical Systems. It interfaces directly with Varian's treatment planning and dose-delivery equipment.

Since ARIA records both the patient statistics and complete treatment data (including the type and amount of radiation delivered, field size, and gantry angle), it is a very useful tool for accurate determination of the true workload and barrier usages of each treatment room. As an example, Figure 4.4 shows a plot of the number of Monitor Units[1] (MUs) generated by the Clinac 21EX-A linear accelerator as a function of gantry angle over the course of a single year. From this plot, the workload of the machine and the usage factors of the four primary barriers may be determined.

The facilities of the Radiation Oncology department at the MGH are heavily used. Each year, approximately 3 000 patients are provided with radiation therapy. Various personnel are employed directly by the department, including radiation therapists, information technology technicians, and administrative personnel. Patient support in the waiting room is provided by volunteers. Treatment planning, quality assurance and maintenance of the facilities is the responsibility of a team of clinical medical physicists and service engineers employed in the Department of Medical Physics at the MGH. Radiation oncology physicians together with radiation oncology residents provide clinical practice in the department.

[1] At the MGH, 1 MU is set to provide a dose to water of 1 cCy at a depth of 10 cm with a source-to-surface distance of 100 cm and a field size of 10 cm $\times$ 10 cm.

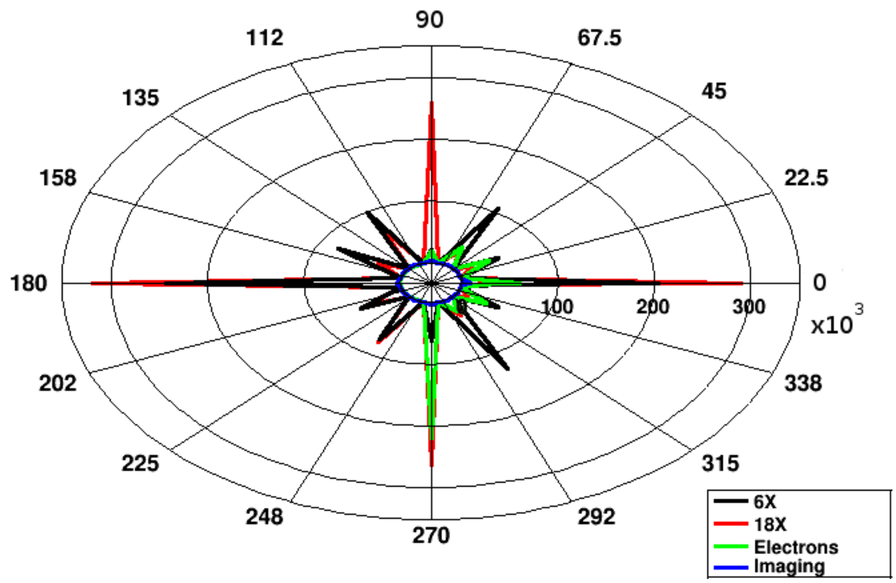

Figure 4.4: Polar histogram of the number of treatment-delivered MUs produced by the Clinac 21EX-A linear accelerator as a function of gantry angle and per energy/modality over the course of one year (June 2008–June 2009). MUs are represented by radial distance from the origin and gantry angle by angular distance from the abscissa. The large number of electron MUs at 270° is due to TSEI treatments (Reynard et al., 2008) in which the patient stands on a rotating platform near the wall of the room at the 270° gantry angle.

Normal treatment hours are from 8 am until 6 pm, Monday to Friday. As such, the treatment machines are available for medical physics calibration and for research use during evenings and weekends.

4.1.2 Departmental Facilities Used for this Research Project

All seven treatment rooms, including the brachytherapy suite, were used at one point or another during this research project. Out of the eight therapeutic radiation-generating devices available at the MGH, the *Tomotherapy* linear accelerator was alone in not being used—its design was unsuitable for the experimental work encountered. Various phantoms and accessories available within each treatment room were employed, as appropriate.

4.2 Radiation Measuring Equipment

A variety of radiation monitoring instruments (area survey meters and TLDs) were available for this project. Table 4.2 provides a list of the devices used. Each of the survey meters was either calibrated in-house as part of this work (as described in section 4.2.1), or within the last year at the National Research Council's (NRC) standard's laboratory in Ottawa, Ontario. Doses recorded on the TLDs were retrieved using the dosimetry service of Health Canada. As described in section 2.9, each instrument presents particular advantages and disadvantages for the low-dose, high-dose-rate measurements encountered in radiation protection.

4.2.1 Survey Meter Calibration using the Shadow-Block Technique

The shadow-block (also referred to as "shadow cone") calibration technique was used for an in-house calibration of the Victoreen 190I and 450P survey meters. The technique was developed at the MUHC by Evans and Corns (2002) and is used annually to calibrate the survey meters at the MGH.

Detector	Radiation Detected	Detector Type	Model	Serial No.	Last Calibrated
Geiger counter survey meter	X rays/γ rays	Gas-filled	Victoreen 190I	193	August 2009
Ion chamber survey meter	X rays/γ rays	Gas-filled	Victoreen 450P	4395	May 2009
Neutron meter	Neutrons	Gas-filled	Victoreen 190N	1312	June 2009
Spherical ion chamber	X rays/γ rays	Gas-filled	PTW 32003	0108	June 2008
TLDs	X rays/γ rays	TLD	Health Canada	many	n/a

Table 4.2: List of radiation detectors used in this research project.

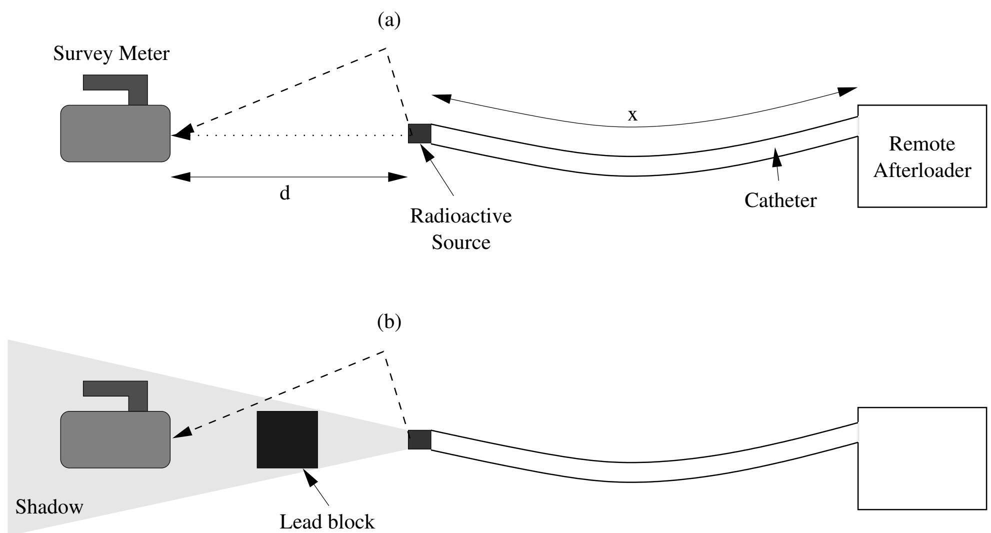

Figure 4.5: Illustration of the shadow-block technique. A survey meter is positioned at distance d from a radioactive source of known air kerma strength. (a) The survey meter is exposed to direct primary radiation (dotted line) and scattered radiation (dashed line) from the source. (b) With a lead block in front of the source, the survey meter is exposed only to the scattered radiation. In both cases, the source travels distance x from the remote afterloader unit to the measurement position through a catheter. The technique facilitates measurement of the primary and scatter components of the radiation reaching the survey meter.

Using the shadow-block technique, a radioactive source of known air-kerma strength may be used to calibrate a radiation detector positioned at a measured distance away. The method is illustrated in Figure 4.5. Accounting for the fall-off in exposure as a function of distance, due to the inverse-square law and attenuation in the intervening medium (air), the exposure reading on the detector may be predicted. The actual reading on the device, however, will be larger than that predicted, owing to radiation scattered off the surroundings and back to the detector. Although very difficult to predict, the scatter component is easily measured by placing a block of attenuating material between source and detector, such that the detector is within the "shadow" of the block and the primary radiation is prevented from reaching the detector. The resulting scatter-subtracted exposure may be compared with the predicted value and hence used to calibrate the detector.

The technique, as carried out at the MUHC, employs the iridium-192 source (nominal activity ∼10 Ci, [37×10^{10} s^{-1}]) used for HDR brachytherapy treatments in the Department of Radiation Oncology (room D5 236 in Figure 4.1 and Table 4.1). The source, welded to the end of a wire, is held within a shielded compartment of a remote afterloader unit (Nucleotron *microSelectron*) when not in use. During patient treatment, the source is driven through a catheter, under computer control, from the shielded compartment to the "dwell position" within the target volume of the patient. For the survey meter calibration, a catheter of length x was used to bring the source to the measurement position, at a distance d from the survey meter, as shown in Figure 4.5.

The survey meter was calibrated in "integration mode", in which total radiation exposure accumulated during a measurement is recorded. Accordingly, it was necessary to subtract from the total reading the exposure accumulated

Shadow Block	Source to Meter Distance (m)	Source Dwell Time (s)	Expected Exposure (mR)	Measured Exposure (mR)	Radiation Components
No	2.5	120.1		20.70	P+S+T (120.1 s)
No	2.5	0.1		1.39	P+S+T (0.1 s)
No	2.5	120		19.31	P+S (120 s)
Yes	2.5	120.1		0.61	S+T (120.1 s)
Yes	2.5	0.1		0.55	S+T (0.1 s)
Yes	2.5	120		0.06	S only (120 s)
n/a	2.5	120	17.96	19.25	P only (120 s)

Table 4.3: Results from calibration of the Victoreen 190I using the shadow-block technique.

as the source travelled through the catheter to and from the measurement position. This was achieved using a zero-duration exposure,[2] whereby the source was brought to the measurement position and immediately retracted. Table 4.3 presents the calibration results—predicted and measured readings on the detector. The detector reading disagreed with the expected value by 7%, and this is considered acceptable for the type of radiation protection measurements undertaken in this project.

4.3 Evaluation of the NCRP 151 Primary and Secondary Barrier Calculations

Evaluation of the NCRP 151 primary and secondary barrier calculations was straightforward. Using the qCAD-measured geometrical data, expected dose rates behind several primary and secondary barriers were predicted and then measured.

Primary barrier measurements were made without a phantom, since (as pointed out in section 3.5) the NCRP primary barrier calculations involve unattenuated primary beams. Phantoms were, however, placed in the beam for all secondary barrier measurements.

[2] In practice a 0.1 second exposure was the minimum exposure allowed by the brachytherapy treatment planning system.

Linac Room	Energy (MV)	Barrier Material	NCRP 151 Prediction (μSv/hr)	Measured Value (μSv/hr)
		Primary Barriers		
D5 228 (1)	6	Concrete	0.14	0.3
D5 228 (2)	6	Concrete	0.2	0.5
D5 228 (1)	18	Concrete	7.53	20
D5 228 (2)	18	Concrete	9.38	1.2
		Secondary Barriers		
D5 228 (3)	6	Concrete	0.12	0.12
D5 228 (4)	6	Concrete	0.02	0.02
D5 436.1 (5)	6	Concrete	2.0	0.8
D5 436.1 (4)	18	Concrete	0.19	0.38

Table 4.4: Primary and secondary barrier dose rate predictions calculated using NCRP 151 and corresponding measured values. Barrier location numbers are shown in Figure 4.1

Table 4.4 presents a list of the primary and secondary barriers studied, the radiation levels measured and the expected radiation levels that were calculated. It is clear that for the primary and secondary barriers, the NCRP 151 report is a useful guide for the level of radiation expected but cannot be relied upon for completely accurate predictions.

4.4 Maze and Door Dose Evaluation

To examine the validity of the NCRP 151 maze and door dose calculations, a series of measurements were made at different distances measured from the door and traveling into the maze for two of the high-energy treatment rooms, the Clinac 21EX-A (D5 228) and Clinac 21EX-B (D5 232) rooms. Figure 4.6 presents a map of the measurement points used. Dose predictions were calculated for each point using qCAD-determined geometrical parameters and the NCRP 151 formalism, as described in section 3.7. Measurements and calculations were carried out for 6 MV photons only. Throughout the measurements, the treatment room door remained open. Leaving the door open allowed for the dose measured at the door to be subsequently used as part of the open-door feasibility study, discussed in chapter 5.

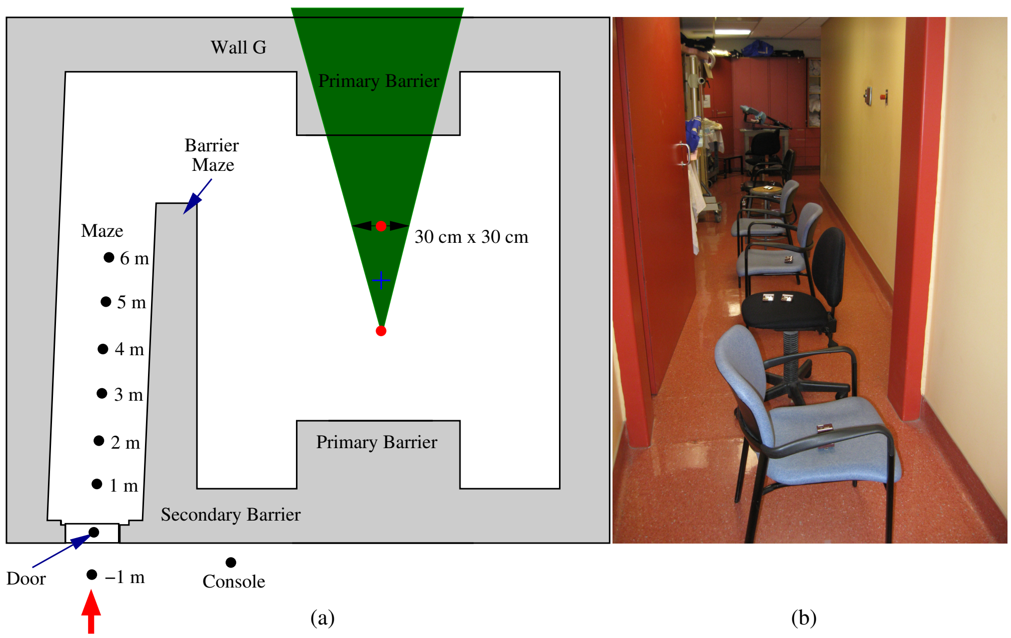

Figure 4.6: Positions at which measurements were made in the evaluation of the NCRP 151 calculations for dose in the maze and at the door. (a) Treatment room plan. Measurement positions are shown along the maze. The location of the isocenter is denoted by a blue cross and the source location by a red dot. The gantry was operated at the 90° angle throughout, with the beam directed onto the wall G. The photograph presented previously in Figure 4.3 corresponds to the gantry setup used. (b) Photograph of the experimental setup for the Clinac 21EX-A treatment room maze, showing TLDs placed on chairs along the maze. The red arrow in (a) shows the photo direction.

Distance from Door (m)	Clinac 21EX-A Predicted (mSv)	Clinac 21EX-A Measured[a] (mSv)	Clinac 21EX-B Predicted (mSv)	Clinac 21EX-B Measured[b] (mSv)
-1 m	0.03	0.15	0.0004	0.000792
Door	0.05	0.24	0.0005	0.00125
1 m	0.07	0.27	0.0006	0.00167
2 m	0.09	0.44	0.0008	0.00252
3 m	0.13	0.64	0.0013	0.00428
4 m	0.2	1.25	0.0021	0.0068
5 m	0.35	2.64	n/a	n/a

[a] Average TLD values for 100 000 MU

[b] Survey meter reading for 10 000 MU

Table 4.5: Predictions for the dose in the maze and at the door using the NCRP 151 formalism and measured values. Due to the maze geometry involved, calculations and measurements were not meaningful for the 5 m position in the Clinac 21EX-B room.

4.4.1 Experimental Procedure

For the measurements made in the Clinac 21EX-A maze, the Victoreen 190I survey meter, operating in integration mode, and 17 TLDs were used. Two TLDs were placed at each of the maze points shown in Figure 4.6 and one TLD was retained at the console. In the Clinac 21EX-B room, two sets of measurements were undertaken, one using the Victoreen 190I only and the second using the Victoreen 450P ionization chamber and TLDs. Both Victoreen devices were operated in integration mode for the 21EX-B measurements. For all measurements, the gantry was rotated to face the wall G, the field size was 30×30 cm^2, and a $30 \times 30 \times 30$ cm^3 solid water phantom was positioned in the beam, its center corresponding with the isocenter. Doses were delivered in irradiations of 10 000 MU each, for a total of 100 000 MU. Between each irradiation the survey meter/ionization chamber was read, zeroed and repositioned. The TLDs remained in place for the full complement of irradiations.

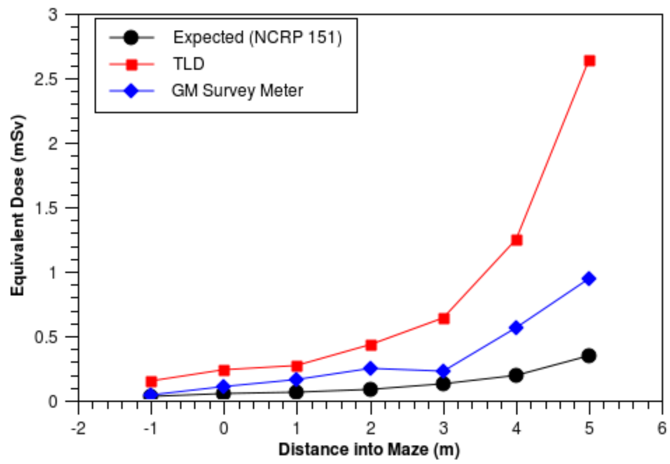

(a) Clinac 21EX-A

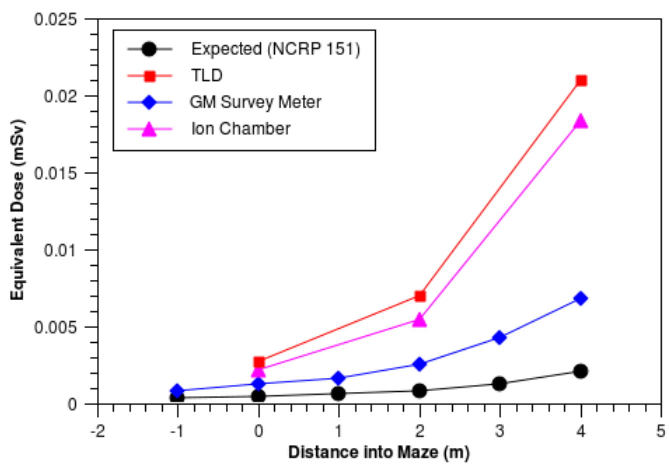

(b) Clinac 21EX-B

Figure 4.7: Measurements and predictions for dose as a function of maze distance for the Clinac 21EX-A and 21EX-B treatment rooms. GM survey meter refers to the Victoreen 190I detector and ionizationionization chamber refers to the Victoreen 450P detector.

4.4.2 Summary of the Maze and Door Results

Table 4.5 summarizes the measurement results along with the corresponding NCRP 151 predictions. Figure 4.7 graphically presents the measurements and predictions.

It is clear from the measurements made in both rooms that the NCRP 151 formalism under-predicts the dose within the maze and at the door. The predictions and measurements disagree by about a factor of five at the door and diverge significantly with increasing distance into the maze. While the level of disagreement at the door is surprising, the divergence down the maze may be attributed to the NCRP 151 calculation conditions (i.e. the acceptable maze height and length ratios discussed in section 3.7.1) no longer holding true.

As was the case for the primary and secondary barrier evaluation discussed earlier, the present results suggest that the NCRP 151 maze and door calculations are useful to the extent that they provide guidance in the design of shielding for radiation therapy treatment rooms but that conservative shielding and actual radiation measurements are essential.

In addition to its usefulness in evaluating the NCRP 151 maze and door dose calculations, Figure 4.7 provides a clear illustration of the inability of a GM tube survey meter to accurately measure high dose rates. In this case, the Victoreen 190I under-performs when compared to both the Victoreen 450P ionization chamber and to the TLD measurements.

4.5 Door Dose as a Function of Gantry Angle

As described in 3.7.1, equal doses delivered to each of the four primary barriers (ceiling, floor, left wall, right wall) does not mean equal doses measured at the door at the end of the maze. Rather, a combined door dose of 2.64 times the wall G dose is predicted by the NCRP 151 report, where wall G is the wall at the end of the maze corridor, opposite the door. Knowing the wall G multiplication factor is useful when measuring the dose at the door and in the maze. Once known, it can be used to convert a measured door dose at the door for wall G to an expected dose at the door for equal doses to the four walls.

To determine the validity of the 2.64 wall-G factor, door dose measurements were made using the Clinac 21EX-A linear accelerator for equal doses delivered to the primary barriers at the four cardinal gantry angles. A dose of 10 000 MU were delivered to isocenter at each angle, for a total of 40 000 MU. The door was open throughout with the door-interlock bypassed. TLDs and the Victoreen 190I survey meter, in integration mode, were used to measure the door dose. None of the TLDs produced readings above the Health Canada reporting threshold. However, using the survey meter, the door dose was measured at 0.03 mSv for the combined 40 000 MU. For the wall G direction (10 000 MU), it registered 0.0135 mSv. The wall-G factor was thus determined to be 2.22. This compares well with the NCRP 151 expectation of 2.64.

CHAPTER 5
Feasibility Study for a Low-energy Open Door Bunker

Radiation therapy treatment rooms containing high-energy linear accelerators (>10 MV) typically incorporate a maze to reduce the neutron flux at the entrance. As discussed in section 3.7, the maze wall eliminates direct neutron irradiation from the entrance and significantly reduces the direct photon flux. Any radiation reaching the door must have undergone at least one scattering, and suffered the consequent reduction in energy, or must have been transmitted, with attenuation, through the maze wall. With the dose at the door significantly reduced, the practical and financial savings in terms of required door thickness are substantial.

For therapy rooms that house dual-energy (below and above 10 MV) linear accelerators, the maze is somewhat otiose during low-energy treatments. However, the presence of the maze suggests an opportunity for leaving the door open during the low-energy treatments.

Open-door treatments are highly desirable from a practical point of view. They allow for speedier treatments (less time spent waiting for the door to open and close), facilitate easier patient access (important in times of patient distress) and reduce wear and tear on the heavily shielded door. However, caution and prudence are required. Before implementation of an open-door treatment policy, it must be demonstrated that any increase in dose at the entrance is compatible with the ALARA principle and well below the legal limits. Furthermore, since the door acts not only as a barrier for shielding purposes but also as an obstacle to entry during treatments, a logical interlock system and a physical deterrent would have to take its place if an open-door policy were introduced for low-energy treatments.

5.1 Low-Energy, Open-Door Proposal for the MGH

In May 2009, following a suggestion by a member of the CNSC (Evans 2009, private communication), it was decided to investigate the feasibility of implementing a policy for low-energy open-door treatments at the MGH. That investigation was subsequently incorporated into this thesis project and is reported here.

Low-energy, open-door treatments are already in operation at the BC Cancer Agency in Victoria, British Columbia. There, the treatment rooms at issue were designed with two-turn mazes such that a door is at all times unnecessary, even for high-energy machines. In practise, however, the Victoria center adopted a conservative approach and implemented a closed-door policy for high-energy treatments and an open-door policy for low-energy treatments. The present proposition for the MGH considers leaving the door of existing single-turn mazes open during low-energy treatments. A retrofitted low-energy open-door policy of this type is already in successful operation at a center in Saskatoon, Saskatchewan (CNSC 2010, private communication).

If implemented at the MGH, the proposed low-energy open-door policy would affect the three mixed-energy treatment rooms: the Clinac 2300 room [1] (D5 426), the Clinac 21EX-A room (D5 228) and the Clinac 21EX-B room

[1] At the time of writing, the Clinac 2300 linear accelerator is being replaced by a Varian Novalis linear accelerator, which will retain the set of treatment modalities previously employed on the Clinac 2300.

(D5 232). The door would be open during monomode[2] and it would remain closed for 18 MV treatments and for mixed 6 MV and 18 MV treatments. Pending further study, it would also initially remain closed during electron treatments. Excluding electrons reduces the complexity of the initial feasibility study. However, given the orders of magnitude lower electron beam current in therapeutic electron beams compared to corresponding photon beams[3] , incorporation of electrons into the policy should pose no major concern at a later date.

5.2 Overview of the Feasibility Study

The feasibility study comprised two parts: (1) an estimation of the expected increase in the dose at the open door using the NCRP 151 formalism, and (2) an accurate measurement of the dose at the door for a realistic simulation of the annual workload, prorated to an experimentally practicable level. The Clinac 21EX-A treatment room was the focus of the feasibility study, with the intention to include the two remaining high-energy treatment rooms at a later date, if appropriate.

[2] Monomode treatments are defined, for the purpose of this work, as radiation therapy treatments involving only a single beam modality of the linear accelerator. Treatments incorporating both 6 MV and 18 MV photons, for example, would not be considered monomode, whereas treatments involving only 6 MV photons would be.

[3] Therapeutic electron beams have low fluxes when compared to therapeutic photon beams since, as shown in Figure 1.1, electron beams reach maximum absorbed dose near the surface and drop quickly to give zero exit dose. Therapeutic photon beams, on the other hand, do not achieve zero exit dose (hence the success of X-ray imaging) and contain what may be considered “wasted” exit dose that must be compensated for by higher entrance dose.

Prior to estimating doses, it was necessary to evaluate the expected workload for the Clinac 21EX-A room and to examine a safe procedure to be used to override the existing door interlocks.

5.2.1 Workload Evaluation

As described in section 3.4, the usefulness of a shielding calculation hinges upon a realistic workload projection. For the Clinac 21EX-A linear accelerator at the MGH, the workload was determined using the data extracted from the ARIA database, discussed earlier in section 4.1.1. The projected workload was estimated from the existing data by assuming that year-to-year the type of treatments performed in the room should not change significantly. The assumption is not expected to hold over the long term, since 6 MV IMRT treatments are gaining in popularity (Webb, 2009). Nevertheless, the workload estimate is conservative as the IMRT field sizes are typically much smaller than those used in conventional non-IMRT procedures. To verify the effect of field size, i.e, the buildup effect, discussed in section 2.8, an experimental field size study was conducted, the results of which are presented in section 5.2.1 below.

The annual workload (over the 12-month period June 2008 to June 2009) for the Clinac 21EX-A treatment room is presented in Table 5.1 for the modalities and energies available. The same data were already graphically presented in Figure 4.4. The graph is a polar histogram of treatment MUs binned in 22.5° gantry-angle bins and separated by photon energy and particle type. It is clear that, in addition to a large number of photon treatments carried out at the cardinal angles, the Clinac 21EX-A machine is used to generate a large number of electron MUs at the 270° gantry angle. These are explained by the use of the room for TSEI treatments (Reynard et al., 2008).

To estimate the workload for which the treatment room door could remain open during 6 MV treatments, additional patient data (hospital patient

Modality	Energy	MUs
MV-Imaging	6 MV	27 595
X rays	6 MV	1 223 221
X rays	18 MV	1 461 337
Electrons	4 MeV, 6 MeV, 9 MeV 12 MeV, 16 MeV	462 400
Total	All (photons and electrons)	3 174 553

Table 5.1: Workload of the Clinac 21EX-A machine/room by treatment modality and energy, as retrieved from the ARIA database for the period June 2008 to June 2009.

ID numbers) were retrieved from the ARIA database with each treatment record and a filtering program, written in C++, was used to separate patients according to the mixture of energies used. The resulting workload plot for patients treated with monomode 6 MV treatments is presented in Figure 5.1. Monoenergetic 6 MV treatments represented about 56% of the total number of 6 MV MUs generated by the Clinac 21EX-A linear accelerator over the year (700 000 MU out of 1 250 000 MU). When all energies and modalities are considered, the 6 MV monomode treatments represent about 22% of the annual workload (700 000 MU out of 3 175 148 MU).

Effect of Field Size on the Dose

The dose buildup effect (described in section 2.8), which is attributed to increased dose scattered to the detector with increasing field size, was examined using the primary beams of the Clinac 6EX-A and Clinac 2300 linear accelerators. The beams were aimed at the most accessible primary barriers and the dose beyond those barriers was measured as a function of field size.

A clear increase in dose as a function of field size was observed. Figure 5.2 presents the results of the measurements. While the buildup effect is evident for each of the beams, it was most significant for the 18 MV beam—a finding that may be ascribed to the greater penetrability of the 18 MV beam in the concrete of the barrier. Using the 2×2 cm^2 field as the narrow beam, and the 40×40 cm^2 field as the broad beam, the buildup factor is ∼37 for the 18 MV

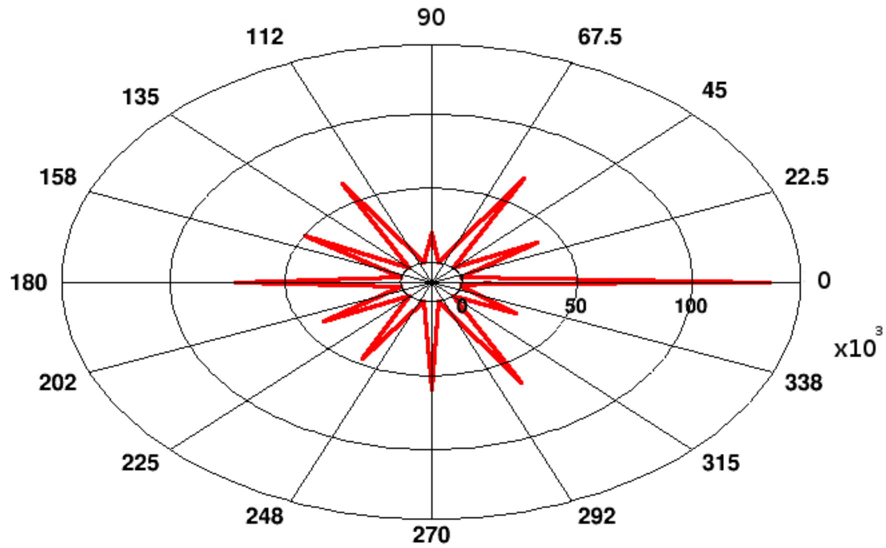

Figure 5.1: Polar histogram of the number of 6 MV monomode treatment-delivered MUs produced by the Clinac 21EX-A linear accelerator as a function of gantry angle over the course of one year (June 2008 to June 2009). MUs are represented by radial distance from the origin and gantry angle by angular distance from the abscissa.

beam and ∼10 for the 6 MV beam. The 6 MV buildup factor is of particular interest in the interpretation of the results of this feasibility study, given that the study incorporated conservatively large field sizes, as is described below.

5.2.2 Treatment Room Door Interlock Override

To properly ascertain the dose at the treatment room door, it was necessary to conduct dose measurements with the door open. Under normal circumstances, an open door triggers multiple safety interlocks in the linear accelerator control system, such that the radiation beam is immediately turned off. Accordingly, it was necessary to override the door interlock.

To achieve the interlock override, the physical sensors (push buttons) in the door frame were manually overridden (depressed) using a metal pole extended across the frame. Several safety precautions were observed. The outer

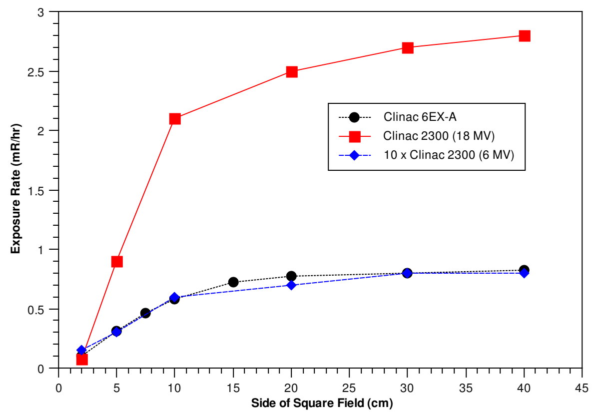

Figure 5.2: Primary beam dose as a function of field size measured outside the primary barriers that shield the Clinac 6EX-A and Clinac 2300 linear accelerators. The clear increase in dose with field size is due to the buildup effect, whereby scattered radiation from broader beams makes its way to the detector. The dose values for the 6 MV beam of Clinac 21EX-A accelerator were very low (since the barrier was designed for 18 MV) and are multiplied by 10 in the plot for clarity.

(wooden) door of the control room was closed and secured to prevent unauthorized access. During measurements, the survey meter was run in integrate mode and left in place at the door or in the maze, while the operators stood at the console and out of the radiation field. A second survey meter with instantaneous readout was retained by the operators. All operators wore TLD badges, as per standard procedure, and all override measurements were logged, as per protocol, in an override logbook kept in the chief engineer's office.

5.3 NCRP 151 Predictions

The NCRP 151 maze and door dose calculations (described in section 3.7) were used to predict the dose at the door for an annual monomode 6 MV workload of 700 000 MU, spread equally over the four cardinal angles of the Clinac 21EX-A treatment room. A summary of the calculations is shown in Table 5.2. Using the NCRP 151 formalism, including the wall-G factor of 2.64, the open-door dose is predicted to be 0.25 mSv per year. This represents the expected increase in dose to a worker if he/she were to stand at the open door throughout the total monomode 6 MV workload of 700 000 MU. It incorporates a conservative field size value of 30×30 cm^2 and does not include the 1/8 door occupancy factor recommended by the NCRP 151 report. As such, it represents a rather conservative estimate.

5.4 Physical Workload Simulation

Given the disagreement between the dose predictions of the NCRP 151 report and experimental measurements, as presented in chapter 4, it was felt prudent not to rely solely on the NCRP formalism to predict the open-door dose expected for monomode 6 MV treatments. Therefore, two physical simulations of the Clinac 21EX-A annual workload were undertaken and actual doses at the door were measured.

5.4.1 Cardinal Angle Simulation

The results of the previously presented (section 4.4), evaluation of the NCRP 151 maze and door dose calculations, were re-examined in the context of measuring the door dose for a physical simulation of the workload spread equally over the four cardinal gantry angles. Specifically, the measurements for the Clinac 21EX-A accelerator (Table 4.5) were analyzed. A dedicated measurement at the (open) door of the Clinac 21EX-B treatment room using TLDs was also undertaken.

For the Clinac 21EX-A, 100 000 MU was delivered to the wall G and a dose of 0.24 mSv was measured at the door. Considering that the experimentally-determined wall-G factor is 2.22 (described in section 4.5), a prorated annual door dose of 0.93 mSv is expected (i.e. for 700 000 MU spread equally over the four cardinal angles). A similar calculation for the Clinac 21EX-B room, using

Quantity	Description	Value	Unit
	General Room Information		
MU	Workload for beam toward Wall G	100 000	MU
W	Workload for beam toward Wall G	1 000	Gy
U_G	Wall G Usage	0.25	
	Beam Energy	6	MV
	Primary Beam Scatter Calculation		
	Composition of primary barrier	Ordinary Concrete	
	Angle of incidence of beam onto area A_0	90	deg
	Angle of reflection of beam off area A_0	82	deg
a_0	Reflection coefficient for first scatter off area A_0	0.0027	
A_0	Area A_0	1.803	m^2
	Angle of incidence for second scatter onto area A_z	90	deg
	Angle of reflection for second scatter off area A_z	89	deg
a_z	Reflection coefficient for second scatter off area A_z	0.008	
A_z	Area A_z	3.59	m^2
d_h	Perp. dist from target to first reflection surface	4.476	m
d_r	Center first refl. surface to maze mid-line	5.524	m
d_z	Center-line distance from point b to maze door	5.723	m
H_S	Dose Equivalent due to primary beam scatter off Wall G	1.75	μSv
	Head Leakage Scatter Calculation		
L_f	Head leakage radiation ratio at 1 m	0.001	
W_L	Workload for leakage radiation	1 000	Gy
U_G	Wall G Usage	0.25	
	Angle of incidence of beam onto area A_1	47	deg
	Angle of reflection of beam off area A_1	0	deg
a_1	Reflection coefficient for scatter of leakage radiation from Wall G	0.0064	
A_1	Area A1	9.86	m^2
d_{sec}	Dist. target to maze center-line at Wall G	7.66	m
d_{zz}	Center-line distance along the maze	8.52	m
H_{LS}	Dose Equivalent due to head leakage scatter	3.70	μSv
	Scatter of Patient Scattered Radiation Calculation		
θ	Angle of patient scattered radiation	47	deg
$a(\theta)$	Scatter fraction for patient scattered radiation	0.0014	
U_G	Wall G Usage	0.25	
W	Workload to Wall G	1 000	Gy
F	Field area at mid-depth of patient at 1 m	900	cm^2
	Angle of incidence onto Wall G, area A1	47	deg
	Angle of reflection from Wall G, area A1	0	deg
a_1	Refl. coef. for Wall G for patient scattered radiation	0.022	
A_1	Area A_1	9.86	m^2
d_{sca}	Distance from target to patient	1	m
d_{sec}	Distance from patient to Wall G at maze center-line	6.95	m
d_{zz}	Distance along maze center-line from Wall G to door	8.52	m
H_{ps}	Dose Equivalent due to scatter of patient scattered radiation	48.33	μSv
	Transmitted Leakage Radiation Calculation		
L_f	Head leakage radiation ratio at 1 m	0.001	
W_L	Workload for leakage radiation	1 000	Gy
U_G	Wall G Usage	0.25	
t_s	Thickness of maze wall traversed	129.7	cm
	Maze wall composition	Ordinary concrete	
TVL_1	For leakage radiation	34	cm
TVL_e	For leakage radiation	29	cm
n	Number of TVLs	4.30	
B	transmission factor for Angle Z along oblique path traced by d_L	0.00005	
d_L	Distance from target to center of maze door through inner maze wall	6.369	m
H_{LT}	Dose Equivalent due to transmitted leakage radiation	0.31	μSv
	Sum of all Contributions		
f	Fraction of primary beam transmitted through patient	0.34	
H_S	Dose Equivalent due to primary beam scatter off Wall G	1.75	μSv
H_{LS}	Dose Equivalent due to head leakage scatter	3.70	μSv
H_{ps}	Dose Equivalent due to scatter of patient scattered radiation	48.33	μSv
H_{LT}	Dose Equivalent due to transmitted leakage radiation	0.31	μSv
H_G	Total dose equivalent at door due to scattered and leakage radiations	52.92	μSv
H_G	Total dose equivalent at door due to scattered and leakage radiations	0.05	mSv
H_{Tot}	Total dose equivalent at door for 100 000 MU to each of 4 cardinal angles (ie 400 000 MU with 2.64 Wall G factor accounted for)	0.14	mSv
H_{annual}	**Prorated annual dose equivalent at door for 700 000 MU**	**0.25**	**mSv/yr**

Table 5.2: Summary of the door dose calculation using the NCRP 151 formalism. A workload of 100 000 MU was used since it corresponded to the dose experimentally delivered as part of the experimental evaluation of NCRP 151, discussed in section 4.4. The final result is prorated for an annual workload of 700 000 MU spread equally over the four cardinal angles.

Beam Direction	MUs	Dose Determination	Measured Dose 21EX-A (mSv)	Measured Dose 21EX-B (mSv)
Wall G	100 000	Experimental	0.24	0.27
Four cardinal angles	400 000	(i.e. 0.24 × 2.22)	0.53	0.59
Four cardinal angles	700 000	Prorated	0.93	1.03

Table 5.3: Calculation of the expected annual dose at the door for the Clinac 21EX-A and Clinac 21EX-B treatment rooms. The calculations use the doses measured for the beams directed to walls G, together with the measured wall-G factors of 2.22 for the Clinac 21EX-A and 2.17 for the Clinac 21EX-B.

a measured door-dose of 0.27 mSv for 100 000 MU to the wall G and an experimentally determined wall-G factor of 2.17, gave an annual dose expectation of 1.03 mSv. Table 5.3 presents the components of the calculations.

5.4.2 Realistic Angular Distribution Simulation

A more realistic physical simulation was achieved through delivery of 70 000 MU toward the walls of the treatment room, using an angular MU distribution weighted according to the angular workload distribution of Figure 5.1. A 30×30 cm^2 field size was used throughout, with a $30 \times 30 \times 30$ cm^3 phantom positioned at the isocenter. Two TLDs were retained at the treatment room door, two at the console and two at the control room door throughout the dose delivery. An integrating survey meter (Victoreen 190I) was read and reset after the prescribed dose was delivered to each of the 12 angles shown in Figure 5.1.

Table 5.4 presents the results of the measurements. The total summed dose registered by the survey meter at the door was 0.0098 mSv, for 70 000 MU generated in the room and spread over the angular distribution of the annual workload. Apart from one TLD, which was retained at the console, no TLDs registered readings above the Health Canada TLD dose reporting threshold of 0.1 mSv. Hence, an upper limit for the door dose read by the TLDs was estimated at 0.1 mSv. When prorated for an annual workload of 700 000 MU,

Gantry Angle (Deg)	MUs	Measured Dose (μSv)
0	14 637	1.73
30	3 973	0.61
60	6 774	1.36
90	1 941	0.39
120	6 351	1.13
150	5 002	0.82
180	7 174	0.88
210	4 056	0.39
240	4 680	0.58
270	5 942	0.72
300	6 528	0.84
330	2 942	0.36
Total	70 000	9.80
Total[a]	700 000	0.098 mSv

Table 5.4: Results of the physical workload simulation for monomode 6 MV treatments using the Clinac 21EX-A accelerator. Accumulated dose was measured at the open door for each gantry angle. The number of MUs delivered at each angle was determined from the angular monomode 6 MV workload distribution for a total of 70 000 MU.

[a] Prorated for an annual workload of 700 000 MU

the above results represent a conservative dose upper limit of 1.0 mSv/yr at the door.

As is the case for the NCRP 151 calculation, the door dose estimates derived from physical simulations do not account for either the 1/8 door occupancy factor or the true field size employed in patient treatments, which is much smaller than the 30 × 30 cm^2 field used.

5.4.3 Dose Considerations for 18 MV Treatments

While the results presented above account for the additional dose expected from open-door 6 MV monomode treatments, they do not quantify dose beyond the closed door expected from 18 MV treatments. Treatments involving 18 MV photons account for about 46% of the total workload (1 461 337 MU out of 3 174 553 MU).

To determine the 18 MV dose, dose measurements were conducted outside the closed door of the Clinac 21EX-A treatment room, for a realistic

Angle (Deg)	18 MV Annual Workload (MU/yr)	MUs Delivered	Measured Photon Dose (μSv)	Measured 18 MV Neutron Dose (μSv)	Annual 18 MV Photon Dose (mSv/yr)	Annual 18 MV Neutron Dose (mSv/yr)	Total 18 MV Dose (mSv/yr)
0	310 388	200	0.053	0.003	0.083	0.0047	0.088
30	16 777	200	0.053	0.003	0.004	0.0003	0.004
60	27 842	1 000	0.209	0.023	0.006	0.0006	0.007
90	257 956	500	0.099	0.020	0.051	0.0103	0.061
120	69 650	200	0.027	0.003	0.009	0.0010	0.010
150	31 049	200	0.046	0.016	0.007	0.0025	0.009
180	319 731	200	0.054	0.010	0.087	0.0160	0.103
210	45 089	200	0.059	0.013	0.013	0.0029	0.016
240	78 901	200	0.066	0.006	0.026	0.0024	0.028
270	262 003	200	0.072	0.003	0.095	0.0039	0.099
300	30 360	500	0.162	0.016	0.010	0.0010	0.011
330	11 591	200	0.061	0.006	0.004	0.0003	0.004
All	1 461 337	3 800	0.961	0.122	0.395	0.0469	0.441

Table 5.5: Photon and neutron doses measured outside the closed door of the Clinac 21EX-A treatment room. A field size of 10 cm $\times$ 10 cm was used. Extrapolated dose values corresponding to the annual workload of the room are provided in the rightmost two columns.

18 MV angular workload distribution. The 18 MV angular workload distribution was presented previously in Figure 4.4. 18 MV photon and neutron doses were measured, using the Victoreen 190I survey meter and the Victoreen 190N neutron meter. A realistic field size of 10 $\times$ 10 cm^2 was used throughout. Results are presented in Table 5.5. The extrapolated annual dose resulting from 18 MV photons and photoneutrons outside the closed door was determined to be 0.44 mSv/yr. The closed-door 6 MV dose rate (for a realistic field size of 10 $\times$ 10 cm^2), corresponding to the 6 MV and MV-imaging component of mixed energy treatments, was also measured and was found to be consistent with background ($\sim$0.13 μR/hr).

Given all the above measurements, a conservative upper limit to the annual dose at the door, for monomode 6 MV treatments performed with the door open and for the remaining treatments performed with the door closed, is estimated at 1.42 mSv (0.98 mSv for 6 MV monomode treatments and 0.44 mSv for the remaining treatments).

CHAPTER 6
Conclusions and Future Work

This research project involved a study of shielding design for radiation therapy installations. The study was divided into two parts. The first part comprised an evaluation of the NCRP 151 design formalism. The second part involved a feasibility study for 6 MV open-door radiation therapy treatments at the Montreal General Hospital.

6.0.4 NCRP 151 Evaluation

The NCRP 151 report is a widely-consulted document that describes a design philosophy and a calculation formalism used in the design of shielding barriers for radiation therapy treatment rooms. Several aspects of the NCRP 151 formalism were studied in this project and were found to produce mixed results when compared to experimental measurements. In some cases, calculations for equivalent dose expectations agreed very well with measurements, in other cases, less so. The results of this work suggest that while the NCRP 151 report is very valuable as a guide in the design of shielding for radiation therapy, its predictions for a new installation should not be merely relied upon but should be thoroughly tested prior to commencement of routine radiation therapy service in a new installation. Indeed, this point is emphasized in the document itself.

Modern radiation therapy is moving toward increasingly accurate dose calculations that rely heavily on Monte Carlo simulations. Future shielding design documents will likely rely heavily on such simulations, particularly for the complex calculation of photon and neutron doses at the door of a treatment room and for the dose attenuated by primary barriers when the build-up effect is significant. Indeed, Monte Carlo simulations are already being employed in treatment room shielding evaluations (Facure et al., 2010; Licea A., 2010). A Monte Carlo shielding study for the treatment rooms at the MGH would be a useful and appropriate future project to follow the present work.

6.0.5 Open Door Feasibility Study

In general, the door of a radiation therapy room consists of thick layers of lead and/or other shielding material and remains shut during patient treatments. The purpose of the door is to control access to the treatment room while simultaneously protecting personnel from the potential harmful effects of radiation during treatments. At a practical level, however, the thick and heavy door presents a cumbersome obstruction between the patient and the radiation therapist. It is slow to open and close, owing to its heavy weight, and it is subject to wear and tear. A proposal to examine the feasibility of open-door monoenergetic 6 MV treatments at the MGH comprised the second part of this research project.

A conservative upper limit for the expected annual increase in equivalent dose at the door was estimated to be 1.0 mSv based on realistic simulations of the expected monoenergetic 6 MV workload. The upper limit is conservative since the field size (30×30 cm^2) used in our study is much larger than that used in realistic treatments. Furthermore, if the 1/8 door occupancy factor, as recommended in the NCRP 151 report, is employed the upper limit is reduced to 0.1 mSv, while still remaining conservative.

Given the low expected increase in door dose with an open door approach, it is considered appropriate to proceed with the feasibility study. The next steps will include examination of the technical changes required to the hardware and software of the linear accelerator unit to implement 6 MV open-door treatments. The changes include a photodiode-based maze-entry sensor and interlock, while maintaining the existing door interlock for all 18 MV treatments.

REFERENCES

Canadian Cancer Society: 2009, *Canadian Cancer Statistics 2009*, Canadian Cancer Society

Daugherty, J. K. and Harding, A. K.: 1983, ApJ **273**, 761

Evans, M. and Corns, R.: 2002, *MUHC internal memo*

Facure, A. et al.: 2010, *To be submitted for publication*

Hall, E. J. and Giaccia, A. J.: 2006, *Radiobiology for the Radiologist*, Lippincott Williams and Wilkins

Heilbron, J. L.: 1981, *Amnerican Journal of Physics* **49**, 223

IAEA: 1998, *IAEA TECDOC Series* 1040

IAEA: 2006, *IAEA Safety Reports Series* 47

ICRP Publication 103: 2007, *Annals of the ICRP*

ICRP Publication 90: 2003, *Annals of the ICRP*

IEC Publication 601-2-1: 1981, *IEC Publications, Geneva*

IPEM: 1997, *Intitute of Physics and Engineering in Medicine Report 75*

Kersey, R. W.: 1979, *Medicamundi* **24**, 151

Kertzman, M. and Sembroski, G.: 1994, *Nuclear Instruments and Methods A* **343**, 629

Licea A.: 2010, *Private Communication*

McGinley, P. and Huffman, K.: 2000, *Radiation Protection Management* **17**, 43

McGinley, P. H., Miner, M. S., and Mitchum, M. L.: 1995, *Physics in Medicine and Biology* **40(9)**, 1467

Mettler, F. et al.: 2009, *Radiology* **253**, 2

NCRP: 2005, *NCRP Publications Report 151*

NCRP Report 116: 1993, *NCRP Publications*

NCRP Report 93: 1987, *NCRP Publications*

Podgoršak, E. B.: 2006, *Radiation Physics for Medical Physicists*, Springer

Rawlinson, J. A., Islam, M. K., and Galbraith, D. M.: 2002, *Medical Physics* **29(4)**, 598

Reynard, E., Evans, M., Devic, S., Parker, W., Freeman, C., Roberge, D., and Podgorsak, E.: 2008, *Journal of Applied Clinical Medical Physics* 9(4)

Schulz-Ertner, D. and Tsujii, H.: 2007, *J Clin Oncol* **25(8)**, 953

Wang, Y. Z., Evans, M. D. C., and Podgorsak, E. B.: 2005, *Medical Physics* **32(9)**, 2899

Webb, S.: 2009, in *WC 2009 IFMBE Proceedings 25/I*, p. 49

Wu, K. and McGinley, P. H.: 2003, *Journal of Applied Clinical Medical Physics* 4(2)